Phase-Field Simulation of Solidification with Moving Solids

by

Jorge A. Vieyra Salas

Submitted to the Department of Materials Science and Engineering
in partial fulfillment of the requirements for the degree of

Master of Science

at the

MASSACHUSETTS INSTITUTE OF TECHNOLOGY

September 2005

Author .....
Department of Materials Science and Engineering
May 18, 2005

Certified by .....
Adam C. Powell IV
Assistant Professor
Thesis Supervisor

Accepted by .....
Gerbrand Ceder
Chair, Departmental Committee on Graduate Students

Phase-Field Simulation of Solidification with Moving Solids

by

Jorge A. Vieyra Salas

Submitted to the Department of Materials Science and Engineering
on May 18, 2005, in partial fulfillment of the
requirements for the degree of
Master of Science

Abstract

This thesis presents a novel methodology for simulating solidification using fluid structure interactions coupled with the phase-field method while allowing for topology changes in the solid-liquid interface with non-stationary solids. This methodology is implemented using a finite difference scheme and a semi-implicit integration method. Pure translation and pure rotation cases are demonstrated and a preliminary simulation of applied shear on a particle is presented. These results demonstrate that the model shows promise for understanding the behavior of various systems like semi-solid metals, polymer mixtures, and moving solids undergoing chemical reactions.

Thesis Supervisor: Adam C. Powell IV
Title: Assistant Professor

Acknowledgments

I would not have been able to complete my graduate work without the help and support of numerous people, and I want to express my gratitude to each of them. Besides the ones mentined in these short paragraphs, there were many, many more that either help me on the long road, gave me inspiration to finish my thesis or just simply support.

My mother, back home in Mexico, has supported me thoughout my academic career, giving me her unconditional love and helping me grow up into a man. This work is dedicated to her, and I thank you for all the sacrifices you have made and to my aunt Myrna which deserves equal mention because she is like my second mother, well kind of.

My advisor, Professor Adam Powell IV, which guided me all the way towards the completion of this thesis and always supported me along these years.

I gratefully acknowledge the help of my friend Jorge Carretero who encouraged me, inspired me, and help me write this thesis.

There are several people at MIT that were of tremendous help giving me their support and feedback. I made a few but very good friends while at MIT, people so incredibly talented I feel lucky to say I know them: Simon Bellemare, Taras Gorishnyy and Bruce Wu. They guided me through more tumultuous times, we share a lot of experiencies and memories that I hope we can share again with each other in the future.

Also, my Mexican friends which either I met here at MIT or are old time friends from Mexico. Raymundo Arróyave who knowingly or unknowingly inspired me and helped me focus on the important things. Jorge Feuchtwanger which I know from undergrad school always helped me in the ways he could and gave me lots and lots of guidelines. Juan Gonzalez and Yeriley Lopez which I know from highschool, I am very grateful that we have kept our friendship for so many years.

And last but not least, to my friends ros and bit which have shown me the true meaning of friendship even with such a great distance between us.

Jorge Vieyra, Cambridge MA May, 2005

Contents

1 Introduction **11**

1.1 Motivation 13

1.2 Challenges 14

1.3 Organization 14

2 Background **15**

2.1 Semi-Solid Metals 15

2.2 Solids with Fluid Structure Interactions 17

2.3 Phase-Field 19

2.3.1 Cahn-Hilliard 20

2.3.2 Allen-Cahn 22

2.3.3 Real vs. Enhanced Interface Thickness 24

2.3.4 Adding Orientation 26

2.4 Fluid-Structure Interactions 29

3 Governing Equations **33**

3.1 Introductory remark 33

3.2 Equations 34

3.2.1 Fluid Flow 34

3.2.2 Solid Particle Growth Kinetics 35

3.2.3 Heat equation 37

3.2.4 Elastic response 37

4 Numerical Implementation **39**

4.1 Finite Difference Discretization of the Governing Equations 40

4.1.1 2D Implementation 40

4.2 Software used 46

4.3 Parameters, initial and boundary conditions 47

5 Numerical Results **49**

5.1 Dentritic Growth 49

5.2 Fluid Flow 51

5.2.1 Uniform velocity field 51

5.2.2 Uniform rotation 55

5.2.3 Shear driving force 55

6 Conclusions **59**

6.1 Future Work 60

List of Figures

1-1 Semi-solid being cut with a spatula like butter. 12

1-2 Change from equiaxed dendrite shape to rosette and to spherical shape, *a) equiaxed dendrite, b), c) sheared forms a rosette structure, d) Almost spherical, e) spheroid* [9]. 13

2-1 Molding process using a semi-solid alloy. 16

2-2 *Left:* Simulation of blood cells field [29] [23]. *Right:* Calculated Langrangian mesh used for each of the blood cells. [12] 18

2-3 In a diffuse interface the transition from liquid to solid is gradual, while in the sharp interface the change is sudden. 23

2-4 Total Energy 24

2-5 Free Energy function. 28

2-6 *Left:* Fixed position dendrite in a flow field [29] [23]. *Right:* 3D dendrite simulation without a flow field [12] 30

4-1 Staggered Mesh 40

4-2 Grid points in a cluster Distributed Array 42

4-3 Schematic of a PETSc Distributed Array. Its filed data are stored as a vector. 46

4-4 Parallel calculation in a 4 node cluster. 47

5-1 Particle growth leading to a faceted shape. $k = 2$, $\Delta H = 0.03$. . . . 50

5-2 Particle growth leading to dendritic shape. $k = 0.0001$, $\Delta H = 0.95$. The field on the left is the phase parameter ϕ and the shade indicates orientation θ 50
5-3 Interface thickness, anisotropy. 51
5-4 Faceted particle growth with uniform velocity $u = 0.05$ 51
5-5 $u = 0.2$ 52
5-6 Stable Dendrite, $u = 0.0005$ 52
5-7 Unstable Dendrite $u = 0.01$ 53
5-8 Unstable Dendrite $u = 0.002$ 53
5-9 Mesh Peclet vs Mesh Fourier 54
5-10 Rotating dendrite, $\omega = 0.05$. The shades indicate orientation of the crystal (θ). 55
5-11 Particle in an sinusoidal velocity field: vector-phase, velocity, vorticity and shear fields. The fields from left to right are: 1) phase parameters ϕ,θ,4)Velocity $\vec{v}$, 3) vorticity ω and 4) strains γ_{xy} and γ_{xx} 57

Chapter 1

Introduction

Dendritic growth is important because dendrites are the basic micro-structural pattern in solidified alloys. The pattern formed during the solidification of a pure material depends on the existing thermal field during cooling. Once this pattern is set, it is difficult to change in the solid state without substantial effort, e.g. through mechanical deformation and heat treatment.

The evolution of dendritic micro-structures is reasonably well understood for pure materials growing into undercooled melts under purely diffusive conditions, i.e. when fluid flow is absent.

Usually aluminum alloys are processed either by casting from the liquid state into a mold or by wrought processes such as rolling, extruding or forging. Recently another process has appeared in which the alloy is processed in the temperature range where it is partially liquid and partially solid. This type of process, also known as Semi-Solid Metal (SSM) casting can provide some significant advantages for producing aluminum alloy parts.

This process takes advantage of the thixotropic behavior of a semi-solid aluminum alloy, meaning that it can be handled as a solid when it is static and flows like a liquid when subjected to shearing forces. The unique properties of thixotropic aluminum alloys are often illustrated by the demonstration in which a semi-solid billet is cut with

Figure 1-1: Semi-solid being cut with a spatula like butter.

an spatula as a bar of butter or ice cream. Because of this behavior, the SSM alloy handling can be automated facilitating transfer from the heating furnace to the mold. During the filling process a shearing force is imposed and will cause the semi-solid alloy to flow like a highly viscous liquid, filling the mold smoothly and without entrapping gases and therefore avoiding the creation of poruses and producing a higher strength part. On the other hand, spraying a molten metal into a die usually leads to high porosity which can be reduced by an expensive Hot Isostatic Pressing process. In addition, because of the high solid content and the significantly lower temperatures involved with SSM casting, shrinkage porosity is also minimized. SSM forming processes have also other advantages, which include lower forming temperatures and elimination of molten metal handling. These result in longer mold life, lower energy consumption and reduction of environmental pollution, respectively.

So, if this process is so good why is it not widely used? The answer would be because it has been difficult to predict the rheological behavior of SSM. We do not know how hard it has to be pushed to make it flow and how hard to keep it flowing with a steady or manageable rate in order to fill the molds reliably without human intervention. So far many empirical relations have arisen, however there is not any valid theory that predicts the SSM behavior accurately.

Dendritic micro-structures, which can occur during the solidification of metals and alloys, result from instabilities at the solid-liquid interface. However, micro-structural observations in semisolid metal processing show a contradictory effect when stirring, i.e. the morphology of a particle changes from dendritic to rosette to spherical as the shear rate increases.

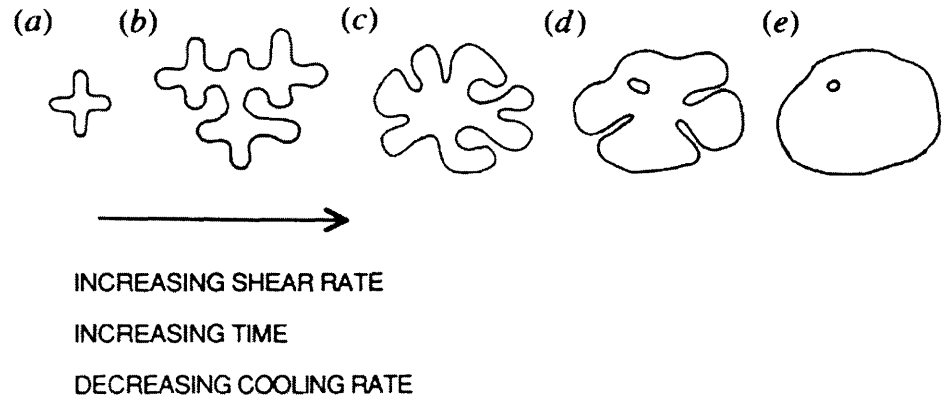

Figure 1-2: Change from equiaxed dendrite shape to rosette and to spherical shape, *a) equiaxed dendrite, b), c) sheared forms a rosette structure, d) Almost spherical, e) spheroid* [9].

1.1 Motivation

Several fundamental questions which are central to their processes have yet to be addressed. The most important such questions are:

- What is responsible mechanism for production of metal spheroids? Is it the dendrite breakage or nucleation in under-cooled liquid?
- If the former, what is the mechanism of dendrite breakage? Is it mechanical fracture, or melting behind the first couple of secondary dendrites?
- Exactly how and why do dendrites in the melt become spheroidal when sheared?

Understanding these phenomena and answering these questions will require great advances in understanding of semi-solid metals, a significant part of which is very

detailed modeling of these solid-liquid systems.

The motivation for this work stems from the need to address these questions and to obtain a more complete picture of the physics involved in the formation of the spherical micro-structure. The aim of this thesis is to develop a framework in which a dendrite could be deformed into a sphere under same conditions in which SSM are formed. The goal of the project is to develop a flexible numerical tool that includes all the of relevant physics involved and to simulate a rotating dendrite being deformed by fluid flow. The wealth of information obtained from such a tool is expected to complement experimental investigations and to some extent help us gain a more complete understanding of this complex process.

1.2 Challenges

Fluid Flow modeling is by itself a very complex and fascinating subject. There is a complete journal and numerous articles in different areas dedicated just to the study of very small aspects of it. It is usually considered a *well studied and known* subject, however there are a lot of intricacies and small details that have to be taken on account which usually are not trivial to handle. Additional complications, such as mass diffusion, particle orientation, heat conduction and deformation of the material, are added to the system, then the complexity and computation time escalates very quickly.

1.3 Organization

In chapter 2 there is a small background of Semi-Solid Metal casting, Phase Field and Fluid Structure Interactions. In chapter 3 the governing equations of the system are explained in detail. In chapter 4 the numerical approximations use to solve this equations are described. And finally chapter 5 shows a few selected cases from these simulations.

Chapter 2

Background

2.1 Semi-Solid Metals

"Semi-Solid forming", also known as "Semi-Solid metallurgy" or "Semi-Solid Metals"(SSM), had been practiced for more than 25 years. The original experiment leading to the invention of SSM was performed in early 1971 by David Spencer as part of his doctoral thesis under M. Flemings supervision at MIT [9]. In that experiment, Spencer discovered the essential rheological properties of vigorously agitated semi-solid metals. Instead of forming a common dendritic micro-structure they formed spheroidal micro-structures. Flemings and Spencer discovered that the non-dendritic nature of the solid phase gave these metal slurries unique rheological properties. They immediately recognized the importance of the discovery and later they demonstrated the feasibility of two routes for producing a SSM. After the discovery of the semi-solid metal microstructure, most part production was done by reheating billets which possessed a suitable microstructure (thixocasting). However, it is now apparent that there are significant advantages of forming semi-solid slurry directly from liquid alloy (rheocasting) and efficient rheocasting processes have been engineered.

Roughly, thixocasting refers to the process of forming billets with spherical microstructures (usually by another company) that can later be reheated and then cast

into the desired mold. Rheocasting is the process in which the semi-solid slurry is made on site and directly cast into the mold skipping the billet step.

The inventors realized that if the metal slurries were formed into parts, the higher viscosity would lead to less turbulent mold filling, thereby producing high quality parts by minimizing the entrapment of air and inclusions. Since then semi-solid metal casting has become a very important process because it opens new possibilities in materials manufacturing, is potentially more economic and leads to better manufactured parts.

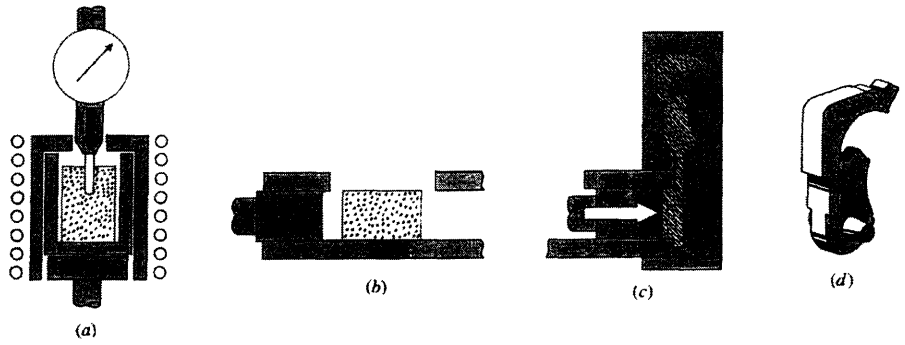

Figure 2-1: Molding process using a semi-solid alloy.

Semi-solid metal casting has yet to take a significant share of the die casting, squeeze casting, and related permanent mold casting markets largely because of the cost of producing the spheroidal micro-structure and difficulty of producing parts with consistent properties. These problems arise because of the use of "thixocasting" instead of "rheocasting", which increases the price because of the inability to recycle scrap on site, such as the metal that is lost due to solidification in the gates and runner. Also the quality cannot be guaranteed because of the inhomogeneity of billet structure and composition. Therefore "rheocasting" is seen as the process that is hoped will solve these issues. If SSM can overcome these limitations, then its advantages of lower solidification shrinkage and lower enthalpy extraction, with consequently less damage to dies and shorter cycle time, have the potential to improve quality and reduce cost of permanent mold castings, and to enable casting of shapes and alloys which are

prohibitively difficult to cast from the liquid state.

Toward that end, the Flemings' group at MIT has been working on new approaches to the production of metals with spheroidal micro-structures. Very recently, their researchers Raul Martinez and James Yurko, have built a device which seems to consistently yield spheroidal micro-structure and a new process has been developed, so progress continues to be made in this area. In their research they have found that the crucial moment when rheocasting a semi-solid metal lies within the initial stages of solidification.

2.2 Solids with Fluid Structure Interactions

One of the challenging aspects of this problem is to couple fluid flow from the melt with the solidifying metal particles or what is known as "Fluid-Structure Interactions". This area in particular has been studied more thoroughly in recent years because of the need to solve systems in which solid particles and the fluid modify each other's behavior, i.e. the particles change the liquid flow path and in turn flow deforms the solid in its path. These interactions require solving both fluid dynamics and solid mechanics of the system simultaneously.

Early pioneers [13] made a substantial contribution in this area which resulted in the widespread use of finite element CFD commercial software packages. Other studies in this subject involved aeroelastic and particle flow modeling [4] as seen in Fig.2-2. However, these studies usually involved the solution of systems of equations in two or more clearly defined domains (as in a solid-liquid system) which had to be coupled at the boundary, the most common of which are the Navier-Stokes equations in a fluid and linear elastic behavior in a solid. This approach is useful for many systems, particularly those which do not suffer any topological changes, such as blood cell damage simulations, pressure waves in flexible tubes, flow in a chemical reactor or airfoil calculations. These kind of problems require the use of a mesh that is calculated at the beginning of the simulation and never changes, as illustrated in Fig.2-2, which

as said previously, are clearly separated and defined. A change in topology would require to refine a new mesh every time such changes arise which could be either a very computational intensive task which would make this calculation unfeasible or in many cases becomes such a complex task that in three dimensions a unsolved problem. People usually refer to this clean separation of interfaces as a *sharp interface*, see Fig.2-3.

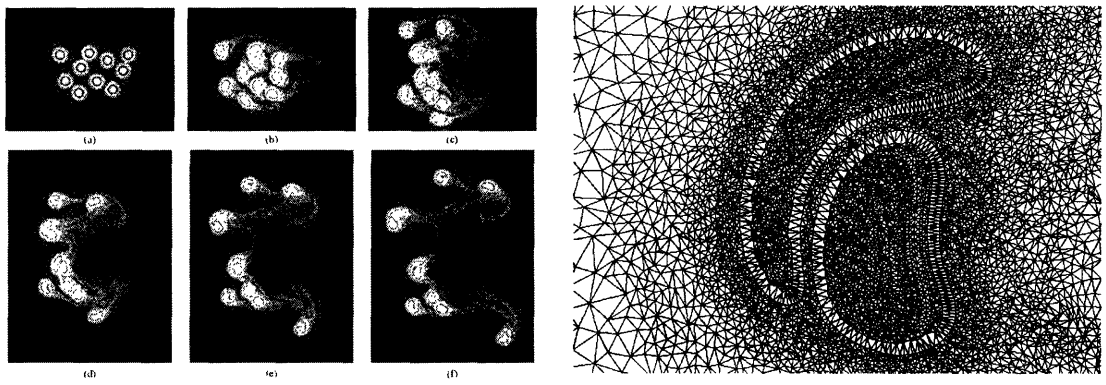

Figure 2-2: *Left:* Simulation of blood cells field [29] [23]. *Right:* Calculated Langrangian mesh used for each of the blood cells. [12]

This difficulty has motivated people to explore metodologies which do not require tracking the interface explicitly in the mesh. Some of them include the level-set method [28] or volume-of-fluid method (VOF) [15] which are used to solve problems involving multi-phase flow with topologically-changing interfaces. Another approach which has raised interest recently is the Phase-Field method, most of which is based on the formalism put forth by either Cahn and Hilliard [6] or Allen and Cahn [1]. From this method a *diffuse interface* arises which allows one to solve the equations as if the system was a single domain, therefore avoiding the need for explicit interface tracking. The use of phase-field is more desirable than the use of other methods because as stated elsewhere [26], interface curvature in a Cahn-Hilliard diffuse interface model is second-order accurate in the mesh spacing as opposed to first-order in VOF, and does not require calculating distance from the interface as level-set methods do; furthermore, when the thermodynamic free energy of a system is well-known, that energy can be incorporated directly into a phase field model. However, the need to

discretize across the diffuse interface, which must be considerably thinner than the smallest lengthscale of the system, renders phase field very computationally intensive.

Prior to the derivation of a model for semi-solid behavior we will present a brief review of some of the modeling and simulation methods that are needed and/or generally used in this field.

2.3 Phase-Field

One of the more popular modeling approaches in solidification is the *Phase Field Method*, which involves building models of phenomena based on thermodynamic "first principles" and simplified kinetic assumptions.

The phase field model has been successfully applied to modeling of dendritic solidification [19]. Warren and others [12][32] have formulated the problem such that crystalline orientation is independent of the coordinate system and discretization grid. Several groups, including Tonhardt *et al.* [30] and Beckermann[29], have solved the Navier-Stokes equations in the liquid phase, and generated 2-D solutions for changes in shape of a stationary dendrite shape in a flow field.

The Phase Field method is of particular interest because it facilitates study of solidification processes. The Phase Field method has been used for two general purposes: to model systems in which the diffuse nature of interfaces is essential to the problem, such as spinodal decomposition and solute trapping during rapid phase boundary motion; and also as a front tracking technique for modeling general multiphase systems, as the ones studied in the present thesis. We generally speak of two types of phase field models. The first one, called Cahn-Hilliard [6] is also referred as Model B or the conserved Ginsberg-Landau equation. In this case, the phase is uniquely determined by the value of a conserved field variable, such as the concentration, e.g. if $C \leq C1$, then we are in one phase, if $C \geq C2$ then the other. These models were first applied to understand spinodal decomposition, and are now used for a wide variety of phenomena, such as phase boundary migration in electrochemistry

[8], polymer membranes [33], electrochemical smelting of titanium . In the second, the Allen-Cahn equation, Model A or the non-conserved Ginsberg-Landau equation, the phase is not uniquely determined by concentration, temperature, pressure, etc., so we add one or more extra field variable(s) sometimes called the order parameter ϕ which determines the local phase. This class of models is widely used to study solidification and solid-state phase transformations in metals.

In the following section we will explain the Cahn-Hilliard Phase-Field model, upon which we will build towards the Allen-Cahn Phase-Field model.

2.3.1 Cahn-Hilliard

In a domain of interest Ω one can calculate the total free energy $\mathcal{F}$ as the integral of a free energy density f_{tot} for a homogeneous system over a body as:

$$\mathcal{F} = \int_{\Omega} f_{\text{tot}} \mathrm{d}V$$

where f_{tot} is a function of C and takes into account every free energy term in the domain. If we take the Taylor expansion to two terms it gives.

$$f_{\text{tot}}(C, \nabla C) = f(C) + \vec{L} \cdot \nabla C + \nabla C \cdot [K] \cdot \nabla C + ... \tag{2.1}$$

$$\vec{L} = \sum_i \frac{\partial f}{\partial \left(\frac{\partial C}{\partial x_i}\right)} \hat{x}_i \tag{2.2}$$

where is a vector evaluated at zero gradient and $[K]$ is a tensor with components:

$$K_{ij} = \frac{1}{2} \frac{\partial^2 f}{\partial \left(\frac{\partial C}{\partial x_i}\right) \partial \left(\frac{\partial C}{\partial x_j}\right)} \tag{2.3}$$

If there is a center of symmetry in the homogeneous material then $\vec{L}$ will be zero,

otherwise the value of f_{tot} would be different for gradients in opposite directions; and $[K]$ will be a symmetric tensor. Furthermore, if the homogeneous material is isotropic or cubic then $[K]$ will be a diagonal tensor with constant components along the diagonal, which can be set to $\alpha/2$:

$$[K] = \begin{bmatrix} \frac{\alpha}{2} & 0 & 0 \\ 0 & \frac{\alpha}{2} & 0 \\ 0 & 0 & \frac{\alpha}{2} \end{bmatrix}.$$

In this simplified system, we can write the total free energy as

$$\mathcal{F} = \int_{\Omega} \left(\frac{\alpha}{2} |\nabla C|^2 + f(C) \right) \mathrm{d}V. \tag{2.4}$$

The two terms in the integral are commonly referred to as the *gradient penalty* and *homogeneous* terms respectively.

Variational calculus helps one to determine the effect of a change in the concentration distribution. For an infinite system, or one with periodic or Dirichlet boundary conditions, we can define the potential μ as

$$\mu = \frac{\delta \mathcal{F}}{\delta C} = -\alpha \nabla^2 C + f'(C). \tag{2.5}$$

This means that for a small change in the concentration function from C to $C + \delta C$ (where C and δC are both functions of position), the total free energy will change by

$$\Delta \mathcal{F} \simeq \int_{\Omega} \mu \delta C \mathrm{d}V. \tag{2.6}$$

The potential can thus be seen as the driving force for local reduction of C, if μ is large then reducing C will reduce the free energy substantially, and vice versa. Equilibrium is attained when μ takes on the same value everywhere.

Because C is locally conserved, its local value changes according to the divergence

of its flux $\vec{J}$, following Fick's second law:

$$\frac{\partial C}{\partial t} = -\nabla \cdot \vec{J}. \tag{2.7}$$

This conservation equation must be closed by a constitutive equation which relates J to C. Since $\mu = \delta\mathcal{F}/\delta C$, we would expect the flux to go from regions where μ is high to regions where it is low, so to a first approximation we can estimate

$$\vec{J} = -M_C \nabla \mu, \tag{2.8}$$

where M_C is the mobility. In some rare circumstances, higher-order terms in $\nabla\mu$ might be needed; if the mobility is anisotropic, M_C will be a second-rank tensor instead of a scalar.

The overall closed transport equation for time-evolution of C is thus

$$\frac{\partial C}{\partial t} = \nabla \cdot (M_C \nabla \mu). \tag{2.9}$$

Note that because μ is second-order in the concentration in Eq.2.6, and Eq.2.9 is second-order in μ, the overall equation is fourth-order in concentration, so Eq.2.9 expands to

$$\frac{\partial C}{\partial t} = \nabla \cdot \left[M_C \nabla \left(-\alpha \nabla^2 C + f'(C) \right) \right]. \tag{2.10}$$

The gradient penalty and homogeneous free energy terms determine the equilibrium thickness of the diffuse interface as discussed in section 2.3.3.

2.3.2 Allen-Cahn

Allen-Cahn systems employ one or more order parameter field variables to determine the phase, commonly labeled ϕ instead of C, hence the term "phase field". The free energy density f_{tot} again is typically given in terms of ϕ and its gradient, and again expanding to second order with symmetry and isotropy this gives a similar expression

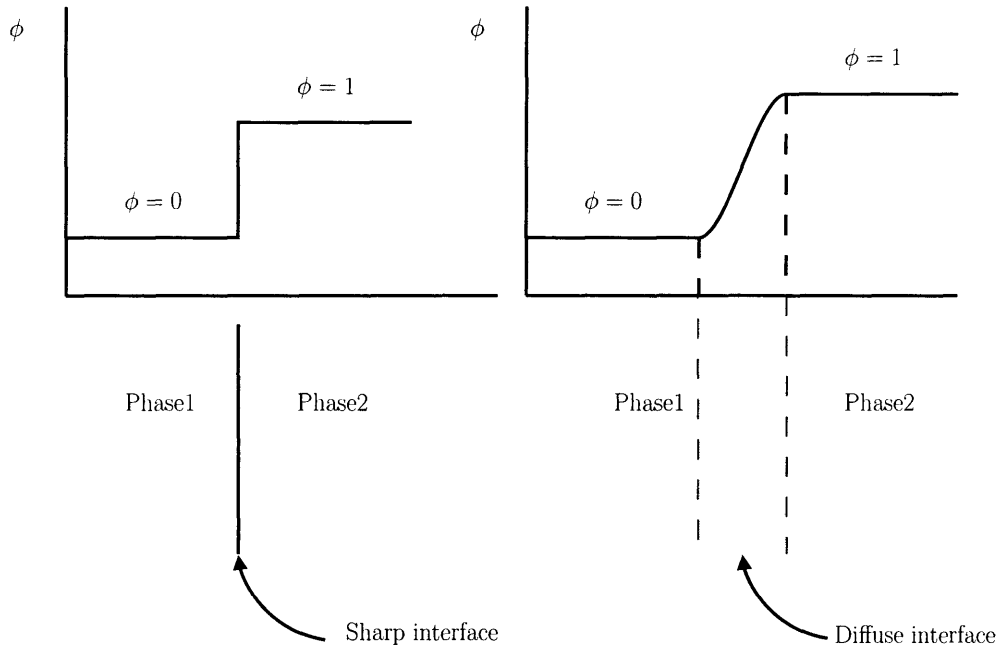

Figure 2-3: In a diffuse interface the transition from liquid to solid is gradual, while in the sharp interface the change is sudden.

as Eq.2.4

$$\mathcal{F} = \int_{\Omega} \left(\frac{\epsilon^2}{2} |\nabla \phi|^2 + f(\phi) \right) \mathrm{d}V. \tag{2.11}$$

Once again $f(\phi)$ is the homogeneous free energy density, typically with local minima at $\phi = 0$ and $\phi = 1$. But this time by convention the gradient penalty coefficient is ϵ^2 instead of α.

Once again one can take the variational derivative of $\mathcal{F}$ with respect to ϕ:

$$\frac{\delta \mathcal{F}}{\delta \phi} = -\epsilon^2 \nabla^2 \phi + f'(\phi). \tag{2.12}$$

Because ϕ is not conserved, instead of using that to determine the flux, we can set the time derivative of ϕ directly to this variational derivative:

$$\frac{\partial \phi}{\partial t} = -M_\phi \frac{\delta \mathcal{F}}{\delta \phi} = M_\phi \left(\epsilon^2 \nabla^2 \phi - f'(\phi) \right). \tag{2.13}$$

Eq.2.13 is what is known as the Allen-Cahn equation or the non-conserved Ginsberg-Landau equation.

2.3.3 Real vs. Enhanced Interface Thickness

For both Cahn-Hilliard and Allen-Cahn, the interface thickness δ and interfacial energy per unit area γ are determined by the competition between the gradient penalty and homogeneous terms in the free energy equations Eq.2.4 or Eq.2.11. If the gradient penalty coefficient is increased, then a thicker interface will minimize the total free energy of the system, and the total energy will be higher as sketched in Figure 2-4, thus both δ and γ will rise with increasing α or ϵ^2. If the free energy for intermediate concentration or order parameter is increased, then a thinner interface will minimize the overall free energy, and the total energy will also be higher, so δ will fall and γ will rise.

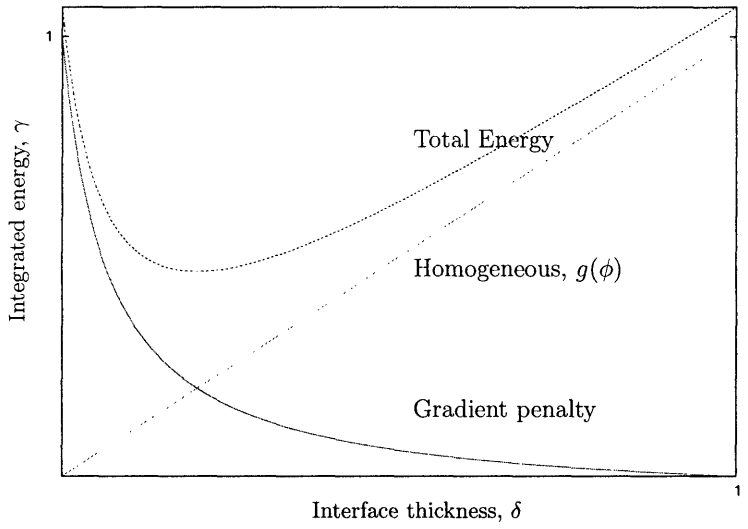

Figure 2-4: Total Energy

In the case of simulations of real structures with diffuse interfaces, because typical real interface thicknesses are on the order of angstroms, the structures modeled tend to be very small, generally on the order of nanometers. As mentioned above, this is useful for modeling phenomena such as spinodal decomposition and solute trapping during solidification. Under these circumstances, we can use the true thermodynamic free energy function for f (to the extent that it exists and is known), and the gradient penalty coefficient α or ϵ is also set to its "real" value, which results in the correct

interfacial energy and equilibrium interface thickness.

To analyze larger systems, one must know something about the homogeneous free energy function f. In Cahn-Hilliard systems, it is customary to write f as the product of a coefficient β and a simple function, *e.g.*

$$f(C) = \beta\Psi(C), \tag{2.14}$$

where $\Psi(C)$ is the double-well function

$$\Psi(C) = 16C^2(1-C)^2. \tag{2.15}$$

β is a scaling factor coefficient related to the peak of the free energy curve.

$$f_{\text{peak}} = \beta\Psi_{\max} = \beta\Psi\left(\frac{1}{2}\right) = \beta \Rightarrow \beta = f_{\text{peak}} \tag{2.16}$$

This results in an equilibrium interface thickness and energy which scales as

$$\delta \sim \sqrt{\frac{\alpha}{\beta}} \quad \text{and} \quad \gamma \sim \sqrt{\alpha\beta}. \tag{2.17}$$

For details on this see Cahn [7].

We can thus use these two parameters α and β to independently set the interfacial energy and thickness. Typically, γ is generally set to its "real" value in the actual system, and δ enhanced by proportionally increasing α and decreasing β, to give a considerably larger interface thickness than that of the actual system. This is because the diffuse interface must be discretized in order to model it accurately. Thus in order to make the discretization as coarse as physically reasonable, δ is chosen to be as large as possible while remaining significantly smaller than the smallest length scale in the model, which is typically a diffusion length.

Likewise, for Allen-Cahn, the dynamics are different but the equilibrium behavior is roughly the same. If the homogeneous free energy is a double-well given by $\beta\Psi(\phi)$

(using Ψ from equation 2.15), then the equilibrium interface thickness and energy are given by

$$\delta \sim \frac{\epsilon}{\sqrt{\beta}} \qquad \text{and} \qquad \gamma \sim \epsilon\sqrt{\beta}. \tag{2.18}$$

2.3.4 Adding Orientation

The Phase-Field Method is useful but still is not exactly what is needed for simulating a semi-solid formation process. By intself the Allen-Cahn formulation does not take into account crystal orientations, grain boundary formation or impingement of the particles. Several authors have extended the model to multiple phases and grain growth. In these models, a finite number of crystalline orientations are allowed with respect to a fixed coordinate reference frame. Before 1998, Morin et al, [24] and Warren et al. [31] constructed the free energy density having N minima by introducing a rotational variable in the homogeneous free energy. Other approaches [22] [16] use different phase variables for every possible orientation (N order parameters for the N allowed orientations [22]. But later it was shown that these approaches were similar. The problem with these approaches was that the free energy density depended on the orientation of the crystal measured in the fixed frame, a property which is not physical.

Later in 1998, Kobayashi, Warren and Carter [20] proposed a vector-valued model for crystallization and grain boundary formation. In this model they provided a description of the growth of independent crystallites and subsequent grain boundary motion. This model improved upon the previous attempts, as it required far fewer equations of motion, and was energetically invariant under rotations. Later, in 2000 [21], they corrected a few inaccuracies in the model, however the revised model for the 2000 formulation requires special numerical treatment. For this reason this project started with the model in the 1998 article with the aim of later implementing the model in the 2000 article and use more accurate physics por the final phases of solidification.

Here is a brief survey of both models in [20] and [21]. The total free energy $\mathcal{F}$

from the previous section.

$$\mathcal{F} = \int_{\Omega} f_{\text{tot}} \mathrm{d}V$$

And we mentioned that f_{tot} is a function that takes into account every free energy term in the domain. If we add a term that takes into account the energy due to orientation mismatch we have the following extended total free energy functional.

$$\mathcal{F} = \int_{\Omega} \left(\frac{\epsilon^2}{2} |\nabla\phi|^2 + sg(\phi)G(\nabla\theta) + f(\phi, T) \right) \mathrm{d}V. \tag{2.19}$$

In the 1998 article [20] it was proposed:

$$\begin{aligned} g(\phi) &= \frac{1}{2}\mu(\phi)\phi^2 \\ \mu(\phi) &= \bar{\mu}\phi^l \qquad\qquad l > 0 \\ G(\nabla\theta) &= |\nabla\theta|^2 \end{aligned} \tag{2.20}$$

Later in the 2000 article [21] it was changed to:

$$\begin{aligned} g(\phi) &= \phi^2 \\ G(\nabla\theta) &= |\nabla\theta| \end{aligned} \tag{2.21}$$

This actually takes into account the impingement in the grain boundary, however it has a singularity, the associated numerical problems require special treatment because they give rise to infinite diffusivity in θ as $\nabla\theta$ approaches to zero.

The variable θ represents the orientation angle of the crystal. In this work we only looked at a 2D simulation, therefore we only needed one angle. However, for a 3D case three angles need to be taken into account.

Furthermore, later it was shown that both linear and quadratic terms are actually needed for a complete description of grain impingement and rotation [32]. The

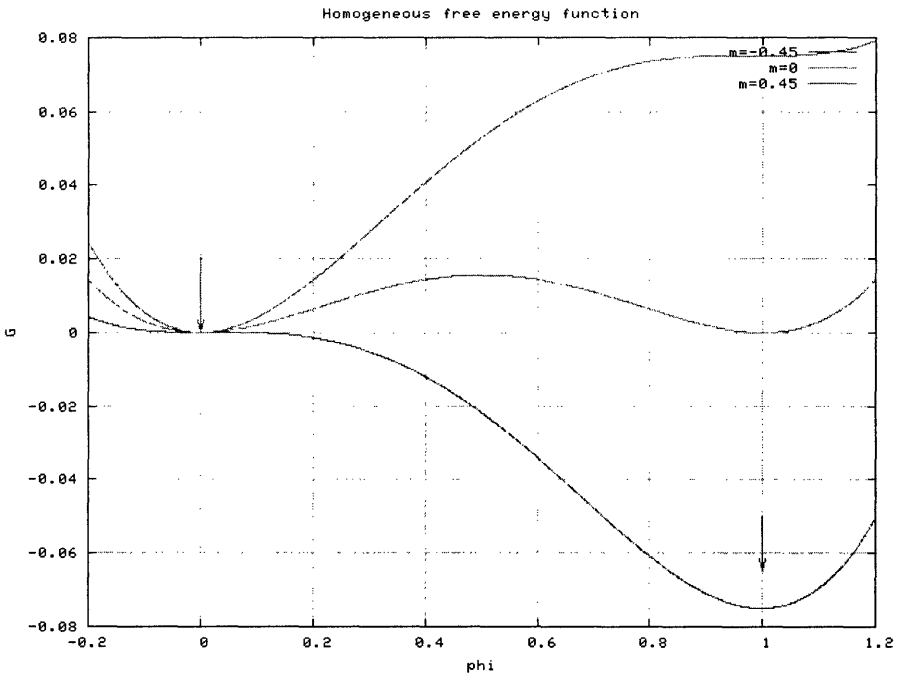

Figure 2-5: Free Energy function.

presence of the linear term $|\nabla\theta|$ is required for grain boundaries that are localized at equilibrium; without this linear term the grain boundary region spreads without bound by relaxational dynamics. In other words, stable grain boundaries of finite width do not exist in the model unless the free energy density models linear dependence on $|\nabla\theta|$. One issue that has to be handled numerically is that the linear dependence on $|\nabla\theta|$ introduces a cusp into the total free energy density when $\nabla\theta = 0$. On the other hand, as explained in [32], at least one term of higher order than linear is essential for the dynamics to include grain boundary motion, therefore a $|\nabla\theta|^2$ term is included so this can be possible. The total free energy using this would be something like,

$$\mathcal{F} = \int_\Omega \left(f(\phi, T) + \frac{\epsilon^2}{2}|\nabla\phi|^2 + s\phi^2|\nabla\theta| + \frac{\epsilon^2}{2}\bar{\mu}\phi^{2+l}|\nabla\theta|^2 \right) \mathrm{d}V$$

The early stages of particle growth can be described without a linear term in $\nabla\theta$ as in the 1998 formulation, since grain boundaries are not yet formed and no

impingement is present. The natural variable for rotation θ is enough for a 2D simulation of a early-stages of semi-solid formation. However, eventually including the linear term in $\nabla\theta$ is desirable.

2.4 Fluid-Structure Interactions

As described previously, it can be seen that phase-field method is useful because it permits one to solve just one equation for the whole domain whithout the need to regenerate a new mesh. From this a *diffuse interface* arises. However, Fluid-Structure Interactions (FSI) require one to account for different behaviors in the different domains: fluid dynamics for the liquid and solid mechanics for the growing particles. Therefore, this problem has an inherent separation of domains or a *sharp interface* which clearly contradicts the usefulness of phase-field, or any Eulerian interface representation for that matter. Nonetheless the use of phase-field is desirable, for reasons mentioned earlier, it incorporates free energy straightforward and simplifies topology changes which others have used to try to solve this dilemma.

Two approaches can be summarized as:

1. Anderson and McFadden treat solid as a fluid "Extremely high viscosity" and solve the standard Navier-Stokes [3].

2. Tonhard and Åmberg use a forcing term in Navier-Stokes which cancels the velocity in the solid to model growth of stationary metal dendrites in a flow field [30]. Beckerman *et al.* have extended this to three dimensions [23] [29]. But both lack the ability to simulate moving solids.

Towards this end, Anderson and McFadden [2] and Jacqmin [17] [18] have led their application to two-fluid systems, and evaluated their advantages and disadvantages with respect to these others.

David Jacqmin [18] has spelled out the mathematical foundation for the use of the phase field method to model two-phase mixtures in fluid dynamics. He used Cahn-

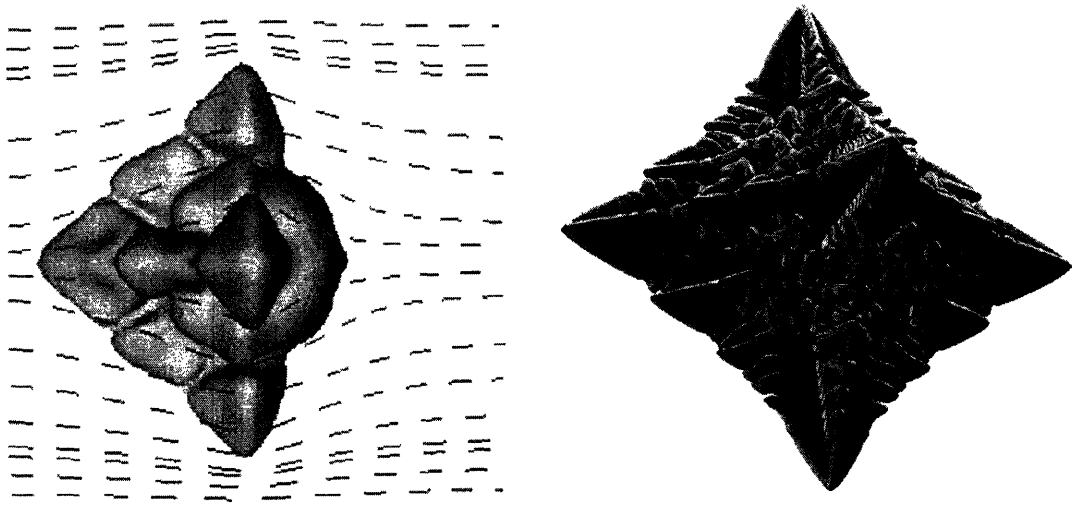

Figure 2-6: *Left:* Fixed position dendrite in a flow field [29] [23]. *Right:* 3D dendrite simulation without a flow field [12]

Hilliard systems and derived forcing terms in the Navier-Stokes equations which give rise to forces equivalent to surface tension (and which are the same as surface tension in the sharp-interface limit). He also analyzed the error with respect to simulation parameters such as resolution and interface thickness.

However because the Phase-Field method is a relatively new approach, traditional fluid-structure interactions models have not been used. Tonhardt and Åmberg [30] and Tong, Beckermann, Karma and Lu [29] [23] have developed a methodology which permits flow past a stationary solid by adding a force term which drives the velocity to zero in the solid, that effectively renders the solid stationary in the fluid. Unfortunately this approach does not allow particles to move in response to flow, nor may multiple particles interact. Anderson, McFadden and Wheeler have modeled a solid as a very viscous fluid in order to approximate interactions between a fluid and a solid [3]. The primary advantage of this method is its simplicity, but it suffers from poor numerical performance and does not represent the constitutive behavior of solids.

Garvin and Udaykumar have developed a similar level-set method [10, 11], their use of only a velocity field with no elastic history in the solid limits its application

to viscoplastic solids, such as metals near their melting point. These approaches can therefore account for only a narrow range of solid constitutive behaviors, and the large difference between the viscosities of the two phases presents computational difficulties. Therefore there were no phase-field formulations with realistic solid constitutive behavior suitable for fluid-structure interaction modeling.

Recently Powell and Dussalt [26] proposed a new mixed-stress model (given later in Eq.3.14) which combines phase-field with fluid-structure interactions while allowing flexibility in the solid consitutive behavior, from elastic to viscoelastic to elastoplastic. A single equation is solved everywhere in the domain and an interpolation function is used to describe the transition between solid and fluid behavior at the diffuse interface.

For this work, Jacqmin's formulation was used as a starting point and similar treatment was derived but for a non-conserved system (Allen-Cahn). The formulation is in two dimensions and the goal is to be able to simulate the system in three dimensions, therefore a preset suitable foundation is necessary.

Chapter 3

Governing Equations

3.1 Introductory remark

A rough description of the modelled system is the following, a liquid phase is set up where a few nuclei are seeded, which grow as the system cools, therefore promoting solid particle growth, as said before a phase-field model with orientation is used to simulate growth. Nucleation kinetics are not to be taken on account due to the differences in time scaling between nucleation and growth rates [14]. Also the heat equation has to be included to account for the released latent heat due to solidification, this will promote the formation of a dendrite. Later, a displacement force is applied on the growing particles so the translate, rotate and deform. This force will affect the heat transfer in the domain of interest due a convective transport. Also, the force will affect the growth of the particles and alter their orientation, deform them and create some strain and change the morphology of the particles. Likewise, the morphology of the solid particles will affect the velocity profiles and therefore change the shear directions along the particle, for this some extra terms are required in the phase-field equations and in the elastic response.

3.2 Equations

3.2.1 Fluid Flow

The Navier-Stokes equations are used to describe fluid flow dynamics. In this case we are assuming incompressible flow and since molten metals behave as a Newtonian fluid viscosity η is to be kept constant. These equations of continuity and motion are give by:

$$\nabla \cdot \vec{v} = 0 \tag{3.1}$$

$$\rho\left(\frac{\partial \vec{v}}{\partial t} + \vec{v} \cdot \nabla \vec{v}\right) = \nabla \cdot \sigma + \vec{g}\rho \tag{3.2}$$

However we are going to use them in a different way because the N-S equations in velocity-vorticity form are easier to solve than in velocity-pressure form, because one do not have to worry about spurrious modes in the pressure field. Also all the necessary terms coupled with the other physical phenomena are included.

$$\frac{\partial \omega}{\partial t} + \vec{v} \cdot \nabla \cdot \omega = \nabla \times (\nabla \cdot \sigma) + \frac{\nabla \times \vec{F}}{\rho} \tag{3.3}$$

$$\nabla^2 u + \frac{\partial \omega}{\partial y} = 0 \tag{3.4}$$

$$\nabla^2 v - \frac{\partial \omega}{\partial x} = 0 \tag{3.5}$$

where:

$$\omega = \nabla \times \vec{v}$$

Eq.3.3 is vorticity time evolution and Eq.3.4 and Eq.3.5 are conservation equations.

3.2.2 Solid Particle Growth Kinetics

As said before, the growth is simulated using Kobayashi, Warren and Carter vector valued phase-field model Eq.[2.19], which is a non-conserved Allen-Cahn type model, with orientation. The field variables can be seen as a order parameter ϕ and orientation θ, or as a vector phase parameter $\vec{P} = (\phi\cos\theta, \phi\sin\theta)$. Starting from Eq.[2.19] for the 1998 formulation:

$$\mathcal{F} = \int_{\Omega} \left(\frac{\epsilon^2}{2} |\nabla\phi|^2 + \mu(\phi)\phi^2 |\nabla\theta|^2 + f(\phi, T) \right) \mathrm{d}V.$$

We first have the homogeneous free energy term, given by

$$f(\phi, T) = -\int_0^{\phi} f'(\phi', m)\, \mathrm{d}\phi' \tag{3.6}$$

where for $|m| < \frac{1}{2}$,

$$f'(\phi, m) = \phi\,(1-\phi)\,(\phi - \frac{1}{2} + m) \tag{3.7}$$

This dependence of f on ϕ and m is shown in figure 2-5. Since m determines the relative stability of the liquid and solid, it is a function of temperature; here this is taken to be,

$$m(T) = \frac{\alpha}{\pi} \tan^{-1} \gamma(T_e - T) \tag{3.8}$$

where, α is a constant < 1 and γ is an energy parameter,T_e is the equilibrium temperature and α is a constant < 1 to prevent $|m|$ from being equal to 0.5, usually is set to $\alpha = 0.9$. If $m > 0$ then the solid phase is stable ($\phi = 1$), likewise if $m < 0$ then the stable phase would be the liquid phase.

The time evolution of the system described above is given by:

$$
\begin{aligned}
\tau\frac{\partial\phi}{\partial t} = -\frac{\delta\mathcal{F}}{\delta\phi} &= \overbrace{-\left\{\nabla\cdot\left[\epsilon\left(\epsilon[I]+\epsilon'[J]\right)\nabla\phi\right]+f'(\phi)-\left[\frac{1}{2}\frac{\partial\mu}{\partial\phi}+\frac{\mu(\phi)}{\phi}\right]|\vec{\beta}|^2\right\}}^{-A} \\
\tau\phi\frac{\partial\theta}{\partial t} = -\frac{1}{\phi}\frac{\delta\mathcal{F}}{\delta\theta} &= \underbrace{-\left\{\frac{1}{\phi}\nabla\cdot\left[\phi\mu(\phi)\vec{\beta}\right]+\frac{\epsilon\epsilon'}{N_0}\frac{|\nabla\phi|^2}{\phi}\right\}}_{-B} \qquad (3.9) \\
\vec{\beta} &= \phi\nabla\theta
\end{aligned}
$$

The matrices $[I]$ and $[J]$ are given by:

$$
[I] = \begin{pmatrix} 1 & 0 \\ 0 & 1 \end{pmatrix}, \qquad [J] = \begin{pmatrix} 0 & -1 \\ 1 & 0 \end{pmatrix}
$$

The vector $\vec{\beta}$ expresses an extent of misorientation which is calculated by

$$
\vec{\beta} = \phi\nabla\theta = -\frac{q}{\phi}\nabla p + \frac{p}{\phi}\nabla q \qquad (3.10)
$$

To couple this with the fluid flow equation, convective terms are added to both parts of Eq.3.9, and rotation to θ equation according to vorticity

$$
\begin{aligned}
\tau\frac{\partial\phi}{\partial t}+\vec{v}\cdot\nabla\phi &= -\frac{\delta\mathcal{F}}{\delta\phi} \qquad (3.11) \\
\tau\phi\frac{\partial\theta}{\partial t}+\vec{v}\cdot\nabla\theta &= -\frac{1}{\phi}\frac{\delta\mathcal{F}}{\delta\theta}+\phi N_0\omega \qquad (3.12)
\end{aligned}
$$

Where:

$$
\vec{v} = (u, v)
$$

Given the above variations, the equations of motion, in terms of the ordering vector $\vec{P} = (p, q) = (\phi\cos\theta, \phi\sin\theta)$

$$\begin{aligned} \tau\frac{\mathrm{D}p}{\mathrm{D}t} &= A\frac{p}{\phi} - B\frac{q}{\phi} \\ \tau\frac{\mathrm{D}q}{\mathrm{D}t} &= B\frac{p}{\phi} - A\frac{q}{\phi} \end{aligned} \tag{3.13}$$

where $\frac{\mathrm{D}}{\mathrm{d}t}$ represents the substantial derivative incorporating convective terms in equations 3.11 and 3.12.

3.2.3 Heat equation

The heat equation describes conservation of thermal energy with conduction and convection taken into account as well as released latent heat which depends on changes in ϕ, the phase parameter. Additionally sometimes an extra term is used to accelerate cooling of the system.

$$\frac{\partial T}{\partial t} + \vec{v}\cdot\nabla T = \frac{k}{\rho C_p}\nabla^2 T + \frac{\Delta H}{C_p}\frac{\mathrm{D}\phi}{\mathrm{D}t} + C(T_{cool} - T)$$

3.2.4 Elastic response

The fluid is subject to viscous stress, while the solid is deformed, like an elastic solid. However the interface is diffuse and has a mixture of liquid and solid behavior. The mixed stress use the simplified form with $\nabla\cdot\vec{u} = 0$ proposed in [26].

This can be summarized as:

$$\begin{aligned} \sigma &= -P[I] - p(\phi)\tau_e - (1-p(\phi))\tau_f \\ P &= -\frac{1}{3}\left(\sigma_{xx} + \sigma_{yy} + \sigma_{zz}\right) \\ \tau_f &= -\eta\left(\nabla\vec{v} + \nabla\vec{v}^T\right) \\ \tau_e &= -G\gamma_e \end{aligned} \tag{3.14}$$

where $p(\phi)$ is an interpolation function to smooth the behavior in the interface such thar $p(0) = 0$ and $p(1) = 1$.

It can be seen that for $\phi = 0$, i.e. in the liquid, Newtonian viscous behavior is obtained:

While where $\phi = 1$ elastic behavior is recovered:

$$\sigma = -P[I] - \tau_f = -P[I] + \eta\left(\nabla\vec{v} + \nabla\vec{v}^T\right) \tag{3.15}$$

$$\sigma = -P[I] - \tau_e = -P[I] + G\gamma_e \tag{3.16}$$

Elastic shear-strain γ_e is a new tensor field with following governing equation:

$$\frac{D}{Dt}\begin{pmatrix}\gamma_{xx}\\ \gamma_{xy}\end{pmatrix} = \begin{pmatrix}2\,\frac{\partial v_x}{\partial x}\\ \frac{\partial v_x}{\partial y} + \frac{\partial v_y}{\partial x}\end{pmatrix} + \begin{pmatrix}-2\omega\gamma_{xy}\\ 2\omega\gamma_{xx}\end{pmatrix} \tag{3.17}$$

To incorporate this into velocity-vorticity $\vec{u} - \omega$, the curl of the divergence is needed, which for contant G is given by:

$$\nabla \times (-\nabla \cdot \tau) = G\nabla \times (\nabla \cdot \gamma) = G\left(\frac{\partial^2\gamma_{xy}}{\partial x^2} + \frac{\partial^2\gamma_{yy}}{\partial x\partial y} - \frac{\partial^2\gamma_{xx}}{\partial x\partial y} - \frac{\partial^2\gamma_{yx}}{\partial y^2}\right). \tag{3.18}$$

The symmetry of the shear strain tensor, and the incompressibility condition ($\gamma_{xx} + \gamma_{yy} = 0$) reduce this easily to a function of just γ_{xx} and γ_{xy}.

Chapter 4

Numerical Implementation

As explained before, the governing equations for a fluid system comprise a set of coupled nonlinear partial differential equations (PDEs). In order to numerically solve this system it has to be discretized. Typical discretization methods for nonlinear PDEs are finite difference methods, finite volume methods, and finite element methods. Whichever method is chosen, the final result is the same, a system of nonlinear algebraic equations which can be solved using linear algebra techniques and numerical methods.

This section describes a procedure for discretizing a system of conservation equations and the numerical procedure for solving the them. The methods described here are given for as general a case as possible. The equations are discretized using the *finite difference* method. Then the resulting nonlinear algebraic equations are solved using a non-linear systems of equations solver based on the Newton-Raphson method. This system of equations generates a matrix equation which also has to be solved, this is done using an iterating procedure known as Krylov-subspace method and Generalized Conjugate Residuals (GCR) method.

An issue that has to be pointed out is that not all of the governing equations are time derivatives this is an extra challenge for solving this set of equations.

4.1 Finite Difference Discretization of the Governing Equations

The uniform mesh for this system is shown in Fig.4-1. Since we are using the velocity-vorticity formulation all of the fields related to fluid flow are placed on the main grid points. For strains a staggered mesh is used. The ω, $\vec{v}$, T, ϕ and θ nodes are at the main grid points, γ_{xx} is shifted to the left and γ_{xy} is shifted down. In order to avoid numerical artifacts, the strains γ_{kk} are taken using a staggered grid. Δx, Δy and Δt are simulation parameters. nx and ny are the numbers of grid points in the x and y directions respectively. Boundary conditions are either periodic or set with a boundary function.

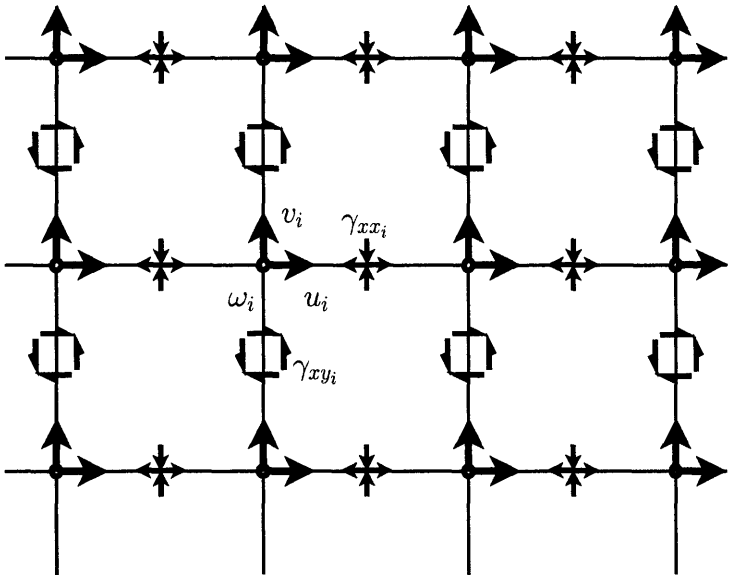

Figure 4-1: Staggered Mesh

4.1.1 2D Implementation

As mentioned before, the equations are solved for the 2D case only. Since the vorticity ω only has one component in the z-direction, we can consider it to be a scalar. Therefore the equations for the 2D case would be as following:

Navier-Stokes:

$$\begin{aligned}\frac{\partial\omega}{\partial t}+u\frac{\partial\omega}{\partial x}+v\frac{\partial\omega}{\partial y} &= Gp(\phi)\left(\frac{\partial^2\gamma_{xy}}{\partial x^2}-\frac{\partial^2\gamma_{xx}}{\partial x\partial y}-\frac{\partial^2\gamma_{xx}}{\partial x\partial y}-\frac{\partial^2\gamma_{xy}}{\partial y^2}\right)\\ &+ \nu(1-p(\phi))\left(\frac{\partial^2\omega}{\partial y^2}+\frac{\partial^2\omega}{\partial x^2}\right)+\frac{1}{\rho}\left(\frac{\partial F_y}{\partial x}-\frac{\partial F_x}{\partial y}\right) \qquad (4.1)\\ \frac{\partial^2 u}{\partial x^2}+\frac{\partial^2 u}{\partial y^2}+\frac{\partial\omega}{\partial y} &= 0 \qquad (4.2)\\ \frac{\partial^2 v}{\partial x^2}+\frac{\partial^2 v}{\partial y^2}-\frac{\partial\omega}{\partial x} &= 0 \qquad (4.3)\end{aligned}$$

Heat:

$$\begin{aligned}\frac{\partial T}{\partial t}+u\frac{\partial T}{\partial x}+v\frac{\partial T}{\partial x} &= \frac{k}{\rho C_p}\left(\frac{\partial^2 T}{\partial x^2}+\frac{\partial^2 T}{\partial y^2}\right)+\frac{\Delta H}{C_p}\frac{\partial\phi}{\partial t} \qquad (4.4)\\ &+ C(T_{cool}-T)\end{aligned}$$

Vector-valued Allen-Cahn phase field:

$$\begin{aligned}\tau\frac{\mathrm{D}p}{\mathrm{D}t} &= A\frac{p}{\phi}-B\frac{q_i}{\phi_i} \qquad (4.5)\\ \tau\frac{\mathrm{D}q}{\mathrm{D}t} &= A\frac{q}{\phi}+B\frac{p_i}{\phi_i} \qquad (4.6)\end{aligned}$$

$$\begin{aligned}\vec{\beta} &= \phi\nabla\theta=\left(-\frac{q}{\phi}\frac{\partial p}{\partial x}+\frac{p}{\phi}\frac{\partial q}{\partial x},-\frac{q}{\phi}\frac{\partial p}{\partial y}+\frac{p}{\phi}\frac{\partial q}{\partial y}\right) \qquad (4.7)\\ A &= \frac{\partial}{\partial x}\left(\epsilon^2\frac{\partial\phi}{\partial x}-\epsilon\epsilon'\frac{\partial\phi}{\partial y}\right)+\frac{\partial}{\partial y}\left(\epsilon\epsilon'\frac{\partial\phi}{\partial x}+\epsilon^2\frac{\partial\phi}{\partial y}\right)\\ &+ f'(\phi)-\left[\bar{\mu}(l+\frac{1}{2})\phi^{l-1}\right]|\vec{\beta}|^2 \qquad (4.8)\\ B &= \frac{1}{\phi}\nabla\cdot\left(\bar{\mu}\phi^{l+1}\vec{\beta}\right)=\frac{\bar{\mu}}{\phi}\left[\frac{\partial}{\partial x}(\phi^{l+1}\beta_x)+\frac{\partial}{\partial y}(\phi^{l+1}\beta_y)\right] \qquad (4.9)\end{aligned}$$

Shear-strain:

$$\begin{aligned}\frac{\partial\gamma_{xx}}{\partial t}+u\frac{\partial\gamma_{xx}}{\partial x}+v\frac{\partial\gamma_{xx}}{\partial y} &= 2\frac{\partial u}{\partial x}-2\omega\gamma_{xy} \qquad (4.10)\\ \frac{\partial\gamma_{xy}}{\partial t}+u\frac{\partial\gamma_{xy}}{\partial x}+v\frac{\partial\gamma_{xy}}{\partial y} &= \frac{\partial u}{\partial y}+\frac{\partial v}{\partial x}+2\omega\gamma_{xx} \qquad (4.11)\end{aligned}$$

The derivatives were taken using finite differences from the uniform grid. The numerical approximations of fist derivatives were done with central differencing except for differences for the convection terms, the difference was taken in the direction of the flow (upwind). The grid was indexed from the bottom left to the upper right corner, from left to right. So if the first row has N_{row} elements the grid node above an arbitrary element i is $i + N_{row}$. For clarity the indexes for the derivatives in de x-direction are given as $i + 1$, which should be read as $x + \Delta x$. Also the derivatives in the y-direction are given as $j + 2$, which should be read as $y + 2\Delta y$ (in the source code it is read as $i + 2 * N_{row}$).

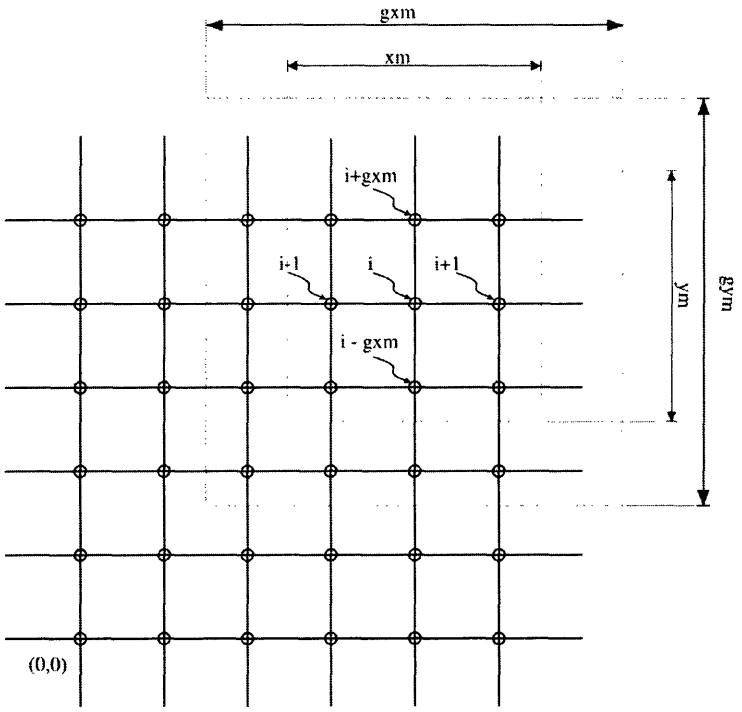

Figure 4-2: Grid points in a cluster Distributed Array

The numerical approximations are the following:

Navier-Stokes:

$$\begin{aligned}\frac{\Delta\omega}{\Delta t} &= -u_i\frac{\omega_i-\omega_{i-1}}{\Delta x}-v_j\frac{\omega_j-\omega_{j-1}}{\Delta y}\\ &+ Gp(\phi_i)\left(\frac{\Delta^2\gamma_{xy}}{\Delta x^2}-\frac{\Delta^2\gamma_{xx}}{\Delta x\Delta y}-\frac{\Delta^2\gamma_{xx}}{\Delta x\Delta y}-\frac{\Delta^2\gamma_{xy}}{\Delta y^2}\right)\\ &+ p(1-\phi_i)\nu\left(\frac{\omega_{i-1}-2\omega_i+\omega_{i+1}}{\Delta x^2}+\frac{\omega_{j-1}-2\omega_j+\omega_{j+1}}{\Delta y^2}\right)+\\ &+ \frac{1}{\rho}\left(\frac{\Delta F_y}{\Delta x}-\frac{\Delta F_x}{\Delta y}\right)\end{aligned} \tag{4.12}$$

and the constraint equations:

$$\frac{u_{i-1}-2u_i+u_{i+1}}{\Delta x^2}+\frac{u_{j-1}-2u_j+u_{j+1}}{\Delta y^2}+\frac{\omega_{j+1}-\omega_{j-1}}{\Delta x} = 0 \tag{4.13}$$

$$\frac{v_{i-1}-2v_i+v_{i+1}}{\Delta x^2}+\frac{v_{j-1}-2v_i+v_{j+1}}{\Delta y^2}-\frac{\omega_{i+1}-\omega_{i-1}}{\Delta x} = 0 \tag{4.14}$$

The chosen interpolation function $p(\phi)$ is an interpolation is:

$$p(\phi)=\begin{cases}0, & \text{if } \phi\le 0.1\\ \frac{1}{0.1215}\left(-\frac{\phi^3}{3}+0.55\phi^2-0.1\phi+\frac{0.29}{6}\right), & \text{if } 0.1<\phi\le 1\\ 1, & \text{if } \phi>1\end{cases} \tag{4.15}$$

Heat conduction:

$$\begin{aligned}\frac{\Delta T}{\Delta t} &= -u_i\frac{T_i-T_{i-1}}{\Delta x}\\ &- v_j\frac{T_j-T_{j-1}}{\Delta x}\\ &+ \frac{k}{\rho C_p}\left(\frac{T_{i-1}-2T_i+T_{i+1}}{\Delta x^2}+\frac{T_{j-1}-2T_j+T_{j+1}}{\Delta y^2}\right)\\ &+ \frac{\Delta H}{C_p}\frac{\Delta\phi_i}{\Delta t}\\ &+ C(T_{cool}-T_i)\end{aligned} \tag{4.16}$$

Vector-valued Allen-Cahn phase field:

$$\tau\frac{\Delta p}{\Delta t} \approx A\frac{p_i}{\phi_i} - B\frac{q_i}{\phi_i} \tag{4.17}$$

$$\tau\frac{\Delta q}{\Delta t} \approx A\frac{q_i}{\phi_i} + B\frac{p_i}{\phi_i} \tag{4.18}$$

$$\begin{aligned} A &\approx \epsilon_i^2\left(\frac{\phi_{i-1}-2\phi_i+\phi_{i+1}}{\Delta x^2}+\frac{\phi_{j-1}-2\phi_j+\phi_{j+1}}{\Delta y^2}\right) \\ &+ f'(\phi_i)+\left[\bar{\mu}(l+\frac{1}{2})\phi^{l-1}\right]|\vec{\beta}|^2 \\ B &\approx \frac{\bar{\mu}}{\phi}\left[(\frac{1}{2}(\phi_{i-1}+\phi_i))^{l+1}\beta_{x+}-(\frac{1}{2}(\phi_i+\phi_{i+1}))_i^{l+1}\beta_{x-}\right]\frac{1}{\Delta x} \\ &+ \frac{\bar{\mu}}{\phi}\left[(\frac{1}{2}(\phi_{j-1}+\phi_j))^{l+1}\beta_{y+}-(\frac{1}{2}(\phi_j+\phi_{j+1}))_i^{l+1}\beta_{y-}\right]\frac{1}{\Delta y} \\ &+ N_0\phi_i\omega_i \\ |\vec{\beta}| &\approx -\frac{\frac{1}{2}(q_i+q_{i+1})\,(p_{i+1}-p_{i-1})}{2\Delta x}+\frac{\frac{1}{2}(p_i+p_{i+1})\,(q_{i+1}-q_{i-1})}{2\Delta x} \end{aligned} \tag{4.19}$$

These equations require the calculation of a few parameters that evolve with time as well but are subidiary equations. These temporary parameters include ϵ, ϕ (since p and q are being used), $\frac{\partial\phi}{\partial t}$, $\frac{\partial\phi}{\partial x}$, $\frac{\partial\phi}{\partial y}$, ψ, $\bar{\psi}$ and $\bar{\theta}$ which are calculated as:

$$\bar{\psi}_i = \tan^{-1}\left(\left(\frac{\partial\phi}{\partial x}\right)_i \Big/ \left(\frac{\partial\phi}{\partial y}\right)_i\right) \tag{4.20}$$

$$\bar{\theta}_i = \frac{1}{N_0}\tan^{-1}\frac{q_i}{p_i} \tag{4.21}$$

$$\psi_i = \bar{\psi}_i - \bar{\theta}_i \tag{4.22}$$

$$\epsilon_i = \epsilon_0\left\{1+\delta_s\left[2\left(\frac{1+\cos N_s\psi_i}{2}\right)^{n_s}-1\right]\right\} \tag{4.23}$$

$$\phi_i = \sqrt{p_i^2 + q_i^2} \tag{4.24}$$

$$\left(\frac{\partial \phi}{\partial x}\right)_i = \phi_{i+1} - \phi_{i-1} \tag{4.25}$$

$$\left(\frac{\partial \phi}{\partial y}\right)_i = \sqrt{p_{j+1}^2 + q_{j+1}^2} - \phi_{j-1} \tag{4.26}$$

$$\left(\frac{\partial \phi}{\partial t}\right)_i = A\frac{\Delta p_i}{\Delta t} - B\frac{\Delta q_i}{\Delta t} \tag{4.27}$$

Because the shear strain is on a staggered mesh, the second derivatives are calculated using four nodes stencil:

$$\left.\frac{\partial^2 \gamma}{\partial x^2}\right|_{x_{1.5}} = \frac{\gamma_0 - \gamma_1 - \gamma_2 + \gamma_3}{2(\Delta x)^2}. \tag{4.28}$$

Shear-strain response:

$$\begin{aligned}
\frac{\Delta \gamma_{xx}}{\Delta t} = & - \frac{1}{2}(u_i + u_{i-1})\frac{\gamma_{xx_{i+1}} - \gamma_{xx_{i-1}}}{\Delta x} \\
& - \frac{1}{2}(v_j + u_{j-1})\frac{\gamma_{xx_{j+1}} - \gamma_{xx_{j-1}}}{2\Delta y} \\
& + \frac{u_i - u_{i-1}}{\Delta x} - \frac{\frac{1}{2}\left((v_j + v_{j+1,i-1}) - (v_{j-1} + v_{j-1,i-1})\right)}{2\Delta y} \\
& - (\omega_i - \omega_{i-1})(\gamma_{xy_j} - \gamma_{xy_{j+1}})
\end{aligned} \tag{4.29}$$

$$\begin{aligned}
\frac{\Delta \gamma_{xy}}{\Delta t} = & - \frac{1}{4}(u_i + u_{i-1} + u_{j-1} + u_{i-1,j-1})\frac{\gamma_{xy_{i+1}} - \gamma_{xy_{i-1}}}{2\Delta x} \\
& - \frac{1}{4}(v_i + v_{i-1} + v_{j-1} + v_{i-1,j-1})\frac{\gamma_{xy_{j+1}} - \gamma_{xy_{j-1}}}{2\Delta y} \\
& + \frac{u_i + u_{i-1} - u_{j-1} - u_{i-1,j-1}}{2\Delta y} + \frac{v_i + v_{i-1} - v_{j-1} - v_{i-1,j-1}}{2\Delta x} \\
& + \frac{1}{4}(\omega_i + \omega_{i-1} + \omega_{j-1} + \omega_{i-1,j-1})(\gamma_{xx_i} + \gamma_{xx_{i-1}})
\end{aligned} \tag{4.30}$$

In the shear-strain equations we are using the notion that $2\frac{\partial u}{\partial x} = \frac{\partial u}{\partial x} - \frac{\partial v}{\partial y}$ since $\frac{\partial u}{\partial x} = -\frac{\partial v}{\partial y}$.

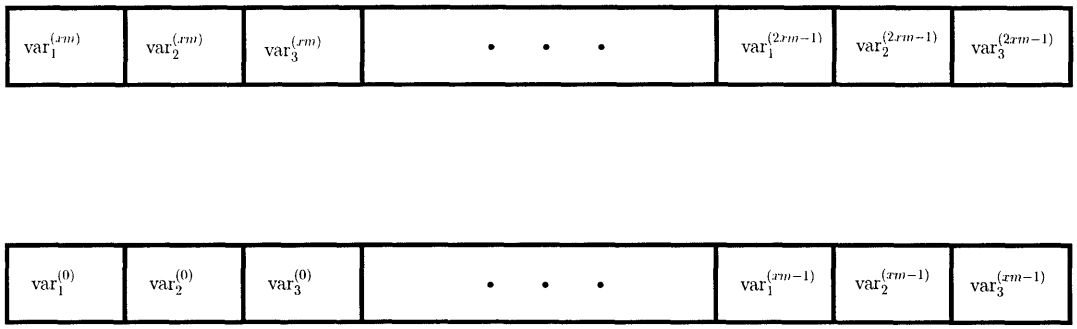

Figure 4-3: Schematic of a PETSc Distributed Array. Its filed data are stored as a vector.

4.2 Software used

To solve this problem a program called `RheoPlast` was written from scratch and is still in development. It is a time stepping software designed to solve multiphysics problems such as this one. It is a continous group effort to have a complete sofware for modeling different types of morphology evolution such as in polymers, electrochemistry and grain growth [27].

RheoPlast uses the "Portable and Extensible Toolkit for Scientific Computation" (*PETSc*) library. *PETSc* is a very powerful general-purpose toolkit which includes state-of-the-art parallel solvers for linear and nonlinear systems of equations, and distributed data objects for finite difference and (under development) finite element discretization of partial differential equations. It has been developed and maintained by a group at Argonne National Laboratories [5].

PETSc proved to be a very useful tool for our purpouses, it let us seamlessly make a calculation either in one machine or a group of them like a cluster.

Also another library *Illuminator*[25] was used for distributed storage. Each node is able to save it's own generated set of data.

The domain is divided and split equally among the processors which receive extra information for the neighboring nodes, this extra points in the mesh are *ghost points* as shown in figure 4-4.

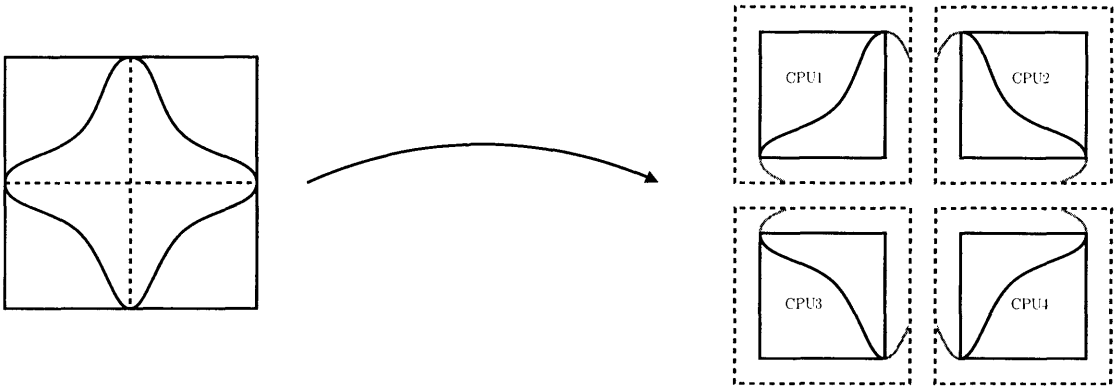

Figure 4-4: Parallel calculation in a 4 node cluster.

4.3 Parameters, initial and boundary conditions

In all simulations, nuclei are placed at random positions with random orientations as initial data, and no nucleation occurs during the simulation. The solid seeds grow with a driving force determined by m. The parameter m in the phase field equations is a function of the temperature T, this is the parameter that controls dendrite formation.

A velocity field is then imposed on the domain: first a uniform velocity field with periodic boundary condition to study the pure translation case then a field such that a constant vorticity is kept throughout the domain and a case where the particle is in pure rotation.

$$\epsilon(\psi) = \epsilon_0 \left\{ 1 + \delta_s \left[2 \left(\frac{1 + \cos N_s \psi}{2} \right)^{n_s} - 1 \right] \right\} \tag{4.31}$$

where:

$$\begin{aligned} N_s &= 4 \\ n_s &= 3 \\ \delta_s &= -0.2; \end{aligned}$$

Chapter 5

Numerical Results

5.1 Dentritic Growth

The dendritic growth in the KWC equation is a behavior that is superimposed on the material that is being simulated. It is an artificial behavior, however is a behavior such that could be tailored to the desired symmetry for specific cases, in this case a 4-fold symmetry is used. Growth anisotropy is given by the function $\epsilon(\psi)$ (Eq.4.31) and plotted in Fig.5-3. This leads to a growth of a faceted particle as seen in Fig.5-1, i.e. like a square, since this it has 4-fold symmetry, this is due to a larger gradient penalty $\epsilon(\psi)$ on the directions normal to the crystal axes and smaller in between such directions.

When the conductivity k is reduced and ΔH is increased, the released heat at the interface inhibits the growth in that direction. Only the fastest growth directions overcome this barrier leading to the formation of a dendritic shape as illustrated in Fig.5-2.

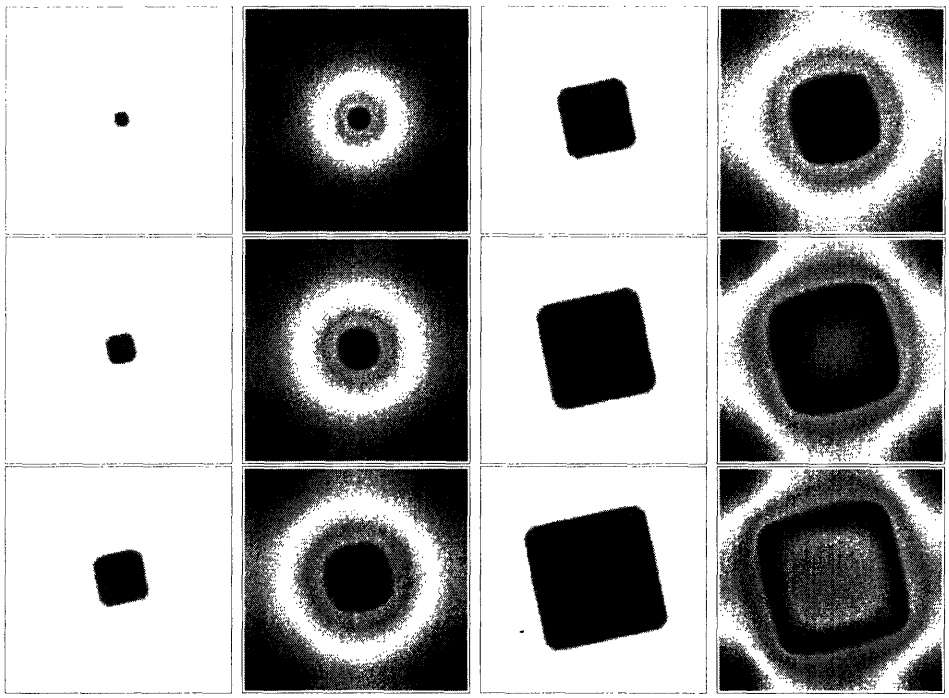

Figure 5-1: Particle growth leading to a faceted shape. $k = 2$, $\Delta H = 0.03$.

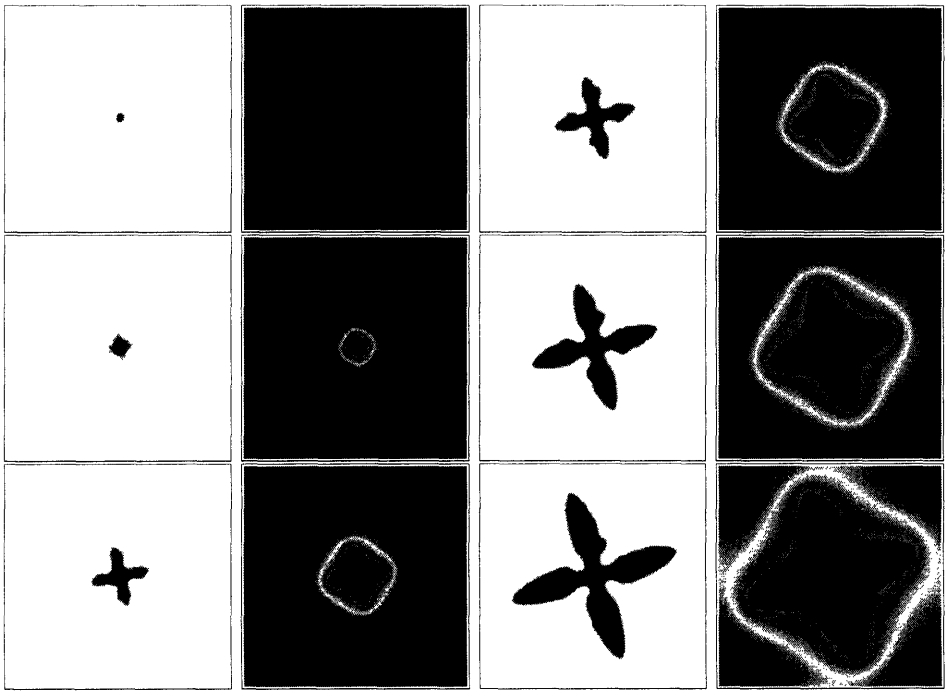

Figure 5-2: Particle growth leading to dendritic shape. $k = 0.0001$, $\Delta H = 0.95$. The field on the left is the phase parameter ϕ and the shade indicates orientation θ

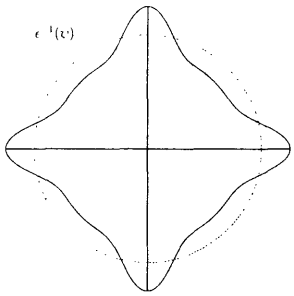

Figure 5-3: Interface thickness, anisotropy.

5.2 Fluid Flow

5.2.1 Uniform velocity field

When a uniform velocity field is applied to the particle, moves accordingly, this is the expected behavior, as shown in Fig. 5-4.

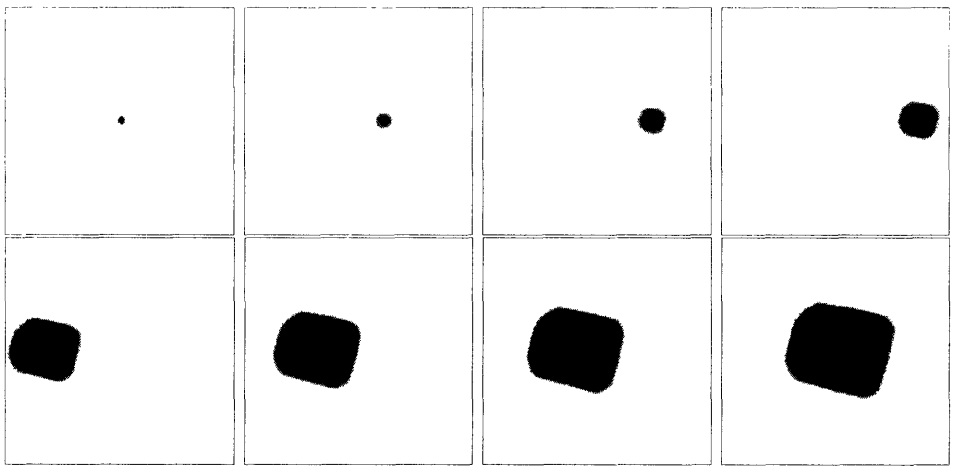

Figure 5-4: Faceted particle growth with uniform velocity $u = 0.05$

However, at larger velocities numerical instability lead to the formation of an oscillating tail. This is probably because of a numerical inaccuracies in the Crank-Nicholson integration method.

This is also true for a dendrite, which is also stable at low velocities. However the instability is amplified allowing stable growth for lower velocities than in the faceted

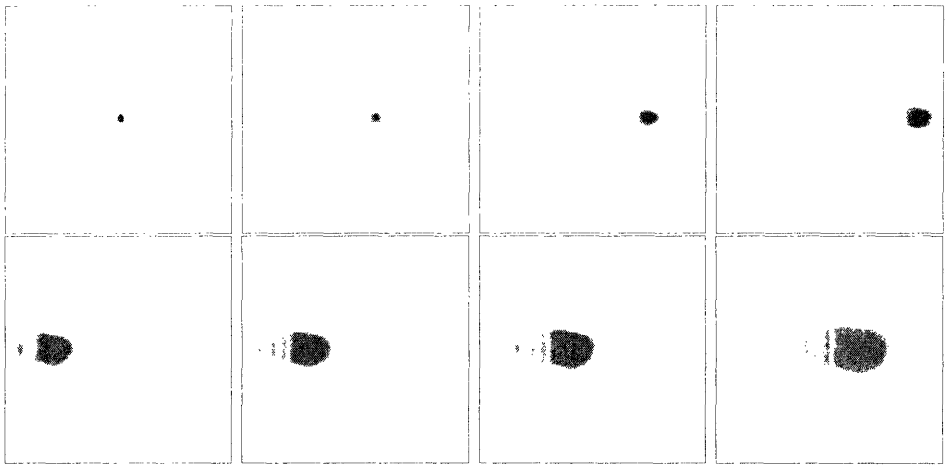

Figure 5-5: $u = 0.2$

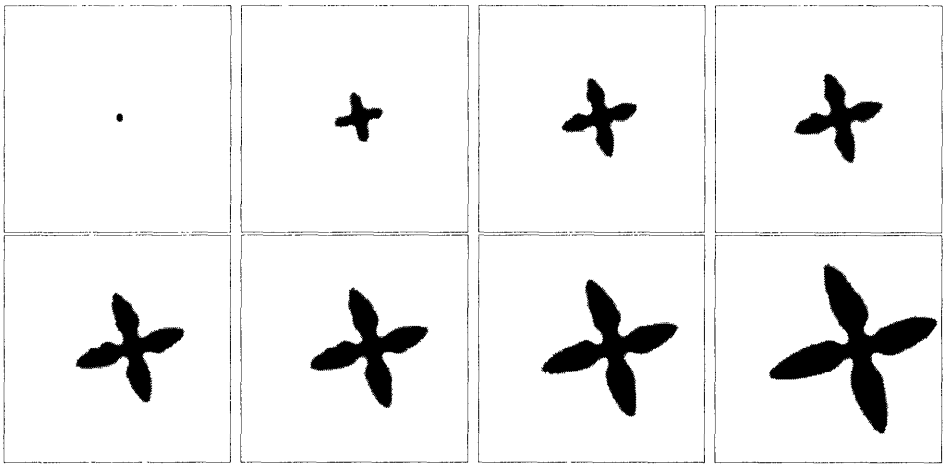

Figure 5-6: Stable Dendrite, $u = 0.0005$

particle case. Even small discrepancies at the beginning of the simulation will lead to a slow particle growth as shown in Fig.5-7 or to a particle with a unrealistic shape, Fig.5-8.

A plot of mesh Peclet number versus mesh Fourier number illustrates the regions for stable particle growth are mapped, this is given in Fig.5-9).

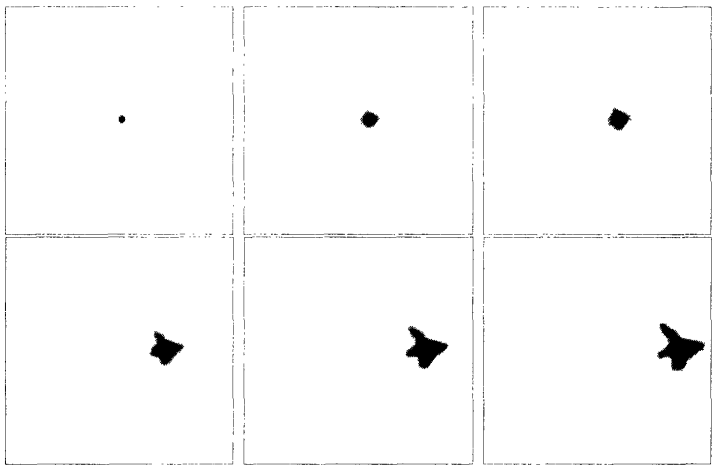

Figure 5-7: Unstable Dendrite $u = 0.01$

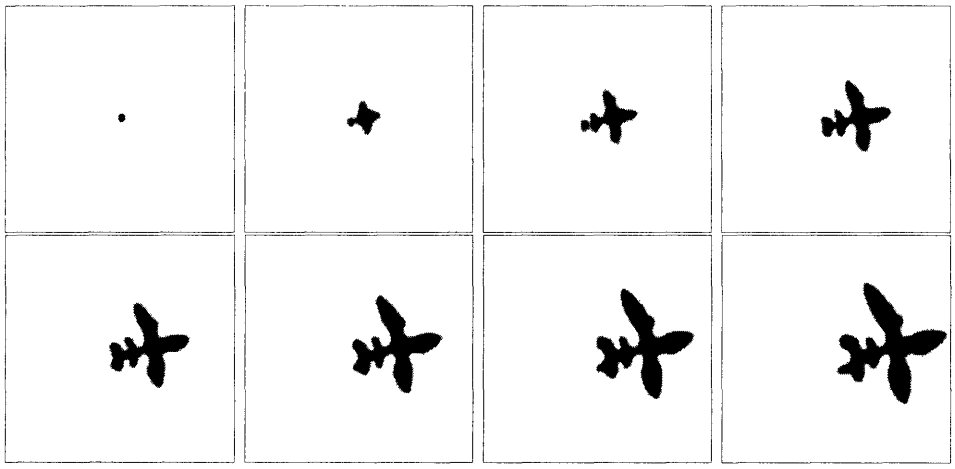

Figure 5-8: Unstable Dendrite $u = 0.002$

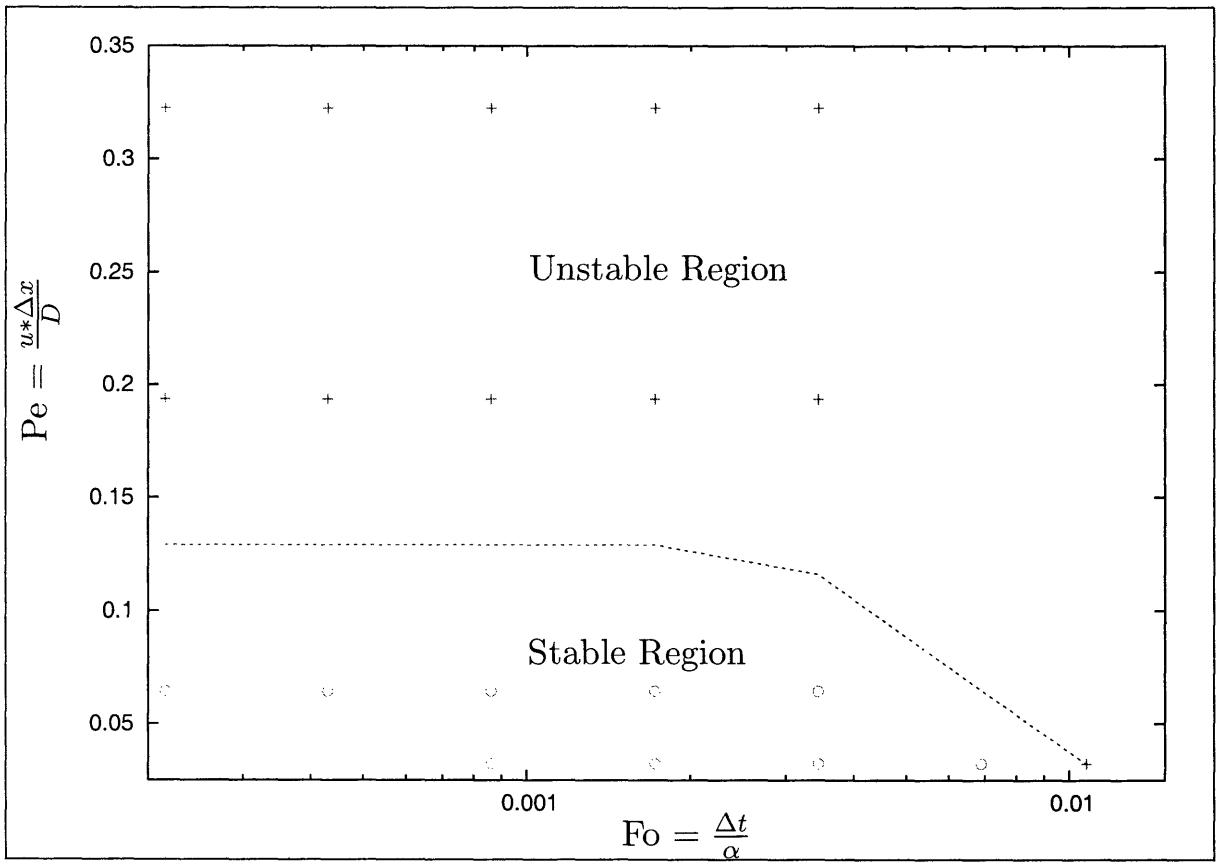

Figure 5-9: Mesh Peclet vs Mesh Fourier

5.2.2 Uniform rotation

If a uniform rotation field is applied to the particle, it rotates with the flow as expected, In this case all the arms are rotating counter-clockwise, therefore in each arm the solid is growing faster on the flow side, which is the expected behavior. The color represents the value of the order parameter θ or the orientation of the crystal as shown in Fig. 5-10.

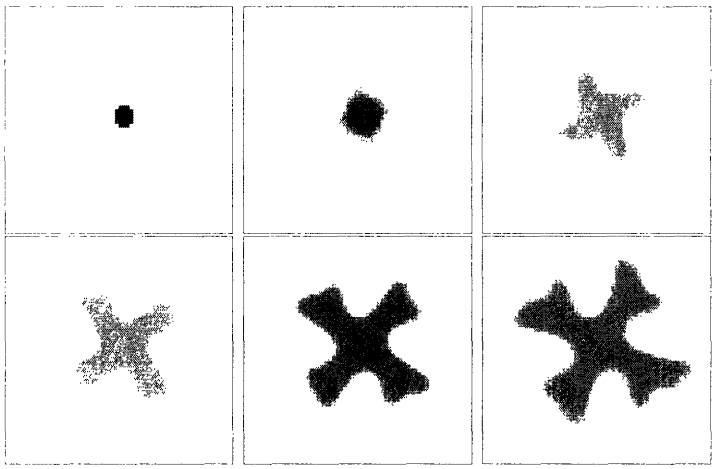

Figure 5-10: Rotating dendrite, $\omega = 0.05$. The shades indicate orientation of the crystal (θ).

We believe that the basic physics are captured in this model. However, the stability region is narrow and this is probably because more resolution is needed in the interface, particularly at the beginning of the simulation when small error in the orientation order parameter will determine the rest of the simulation.

5.2.3 Shear driving force

If the particle is between two driving forces that come from opposite directions it will experience a resultant shearing force. This represents the type of force that a growing particle is subjected to when it is stirred (like in a semisolid). To simulate this kind of behavior a sinusoidal velocity field was applied.

The observed velocity profile is the expected as well as the vorticity field, both

evolve towards the expected behavior, see Fig.5-11. In the strain field this is also the case, the resultant applied shear stress places the particle under a tensional stress at a 45 degree angle, as expected.

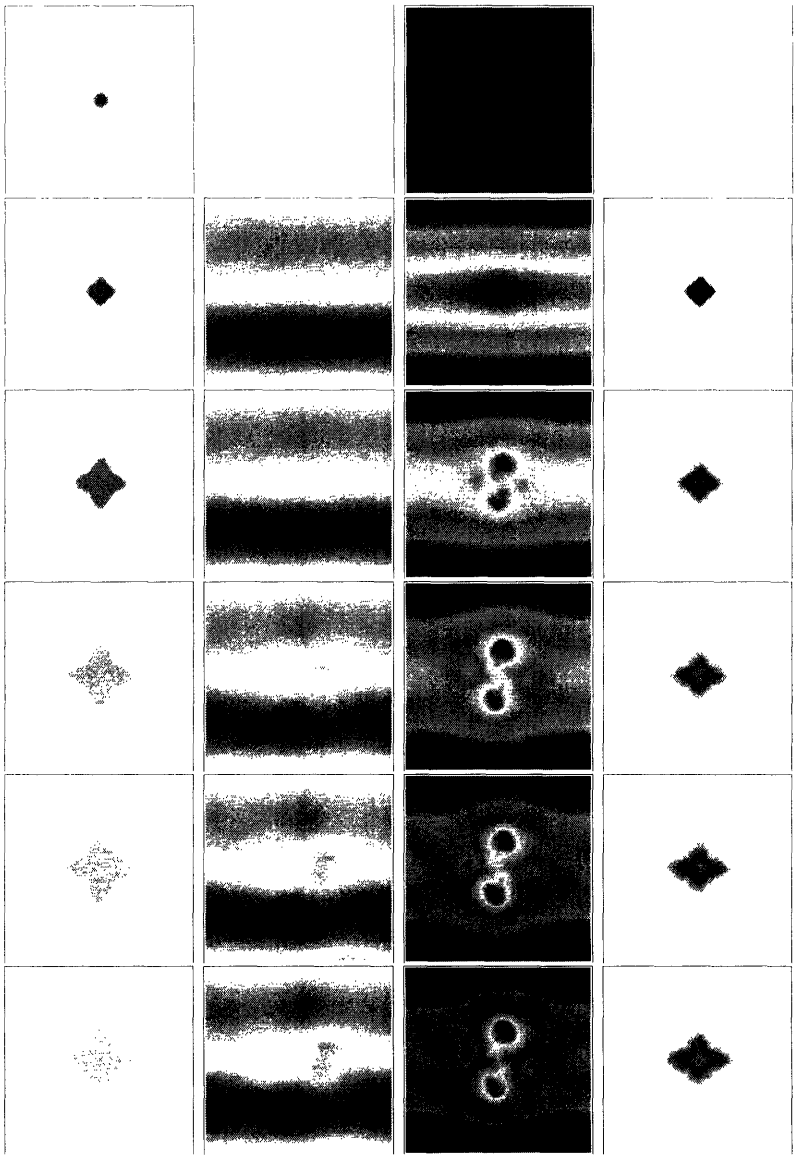

Figure 5-11: Particle in an sinusoidal velocity field: vector-phase, velocity, vorticity and shear fields. The fields from left to right are: 1) phase parameters ϕ,θ,4)Velocity $\vec{v}$, 3) vorticity ω and 4) strains γ_{xy} and γ_{xx}

Chapter 6

Conclusions

Understanding the solidification behavior of moving solids is a key element for a better understanding of the rheological behavior of liquid-solid systems such as semi-solid metals or polymers mixtures.

This effort has developed a promising new method for modeling solidification dynamics with moving solids which addresses this set of problems. Primary findings are summarized as the following:

1. Developed a new method for the simulation of solidification dynamics with moving solids.

2. Implemented this method in a finite difference solution with semi-implicit time-stepping scheme.

3. Demonstrated translation, rotation and preliminary shear results.

4. For translation, demonstrated the correct behavior and characterized growth instability on upwind side of moving particle for different cases with and without dendrites.

5. For rotation, demostrated a quantitatively accurate rotation of orientation order parameter (θ).

6. A preliminary shear stress case was tested, velocity and vorticity follow the expected trends but the model needs further work on stability using a different mesh scheme and Navier-Stokes form.

This represents a promising new method for modelling different systems from semi-solid metals to polymers to a system with chemical reactions.

6.1 Future Work

Finally we include a few recommendations that may be pertinent for anyone who may continue this project. From a modeling perspective the Navier-Stokes equation has been the most challenging one. The current formulation (velocity-vorticity form), although originally deemed advantageous for our 2D simulation, for 3D it may be more problematic than helpful. For this reason we suggest the exploration of alternative formulations (for instance the pressure-velocity form) that may result in a better global behavior and a simpler implementation in 3D. On a separate matter, we believe that a more accurate meshing scheme is necessary. One possibility is to switch to a finite element approach which may be able to enhance the accuracy of the calculations. Ultimately, this code may be extended to a full 3D simulation with which to describe, in detail, the behavior of real systems.

Bibliography

[1] S. Allen and J. Cahn. *Acta Metall. Mater.*, 27:1085, 1979.

[2] D. Anderson and G. McFadden. A diffuse-interface description of fluid systems. Technical Report NISTER 5887, National Institute of Standards and Technology, Gaithersburg, MD, USA.

[3] D. Anderson, G. McFadden, and A. Wheeler. A phase-field model of solidification with convection. *Physica D*, 135:175–194, 2000.

[4] J. Antaki, G. Belloch, O. Ghattas, I. Malcevic, G. Miller, and N. Walkington. A parallel dynamic-mesh lagrangian method for simulation of flows with dynamic interfaces. *Proc. Sci. Comp. 2000*, 2000.

[5] S. Balay, W. Gropp, L. C. McInnes, and B. Smith. Efficient management of parallelism in object oriented numerical software libraries. In E. Arge, A. Bruaset, and H. Langtangen, editors, *Modern Software Tools in Scientific Computing*, pages 163–202. Birkhauser Press, 1997.

[6] J. Cahn and J. Hilliard. *J. Chem. Phys.*, 28:258, 1958.

[7] J. W. Cahn. *Acta Metall.*, 9:795, 1961.

[8] D. Dussault. A diffuse interface model of transport limited electrochemistry in two-phase fluid systems with application to steelmaking. Mechanical engineering s.m. thesis, Massachusetts Institute of Technology, Jan. 2002.

[9] M. Flemings. Behavior of metal alloys in the semisolid state. *Metall. Mater. Trans.*, 22B:269–293, 1991.

[10] J. Garvin and H. Udaykumar. Particle-solidification front dynamics: Part i: Simulations using a fully coupled approach. *J. Crystal Growth*, 252:451–466, 2003.

[11] J. Garvin and H. Udaykumar. Particle-solidification front dynamics: Part ii: The effect of drag laws. *J. Crystal Growth*, 252:467–479, 2003.

[12] W. George and J. A. Warren. *J. Comp. Phys.*, 177:264, 2002.

[13] R. Glowinski, T. Pan, and J. Periaux. Fictitious domain methods for incompressible viscous flow around moving rigid bodies. In *The Mathematics of Finite Elements and Applications*, pages 155–174. John Wiley and Sons, 1996.

[14] L. Gránásy, T. Börzsönyi, and T. Pusztai. *Phys. Rev. Lett.*, 88:206105, 2002.

[15] C. Hirt and B. Nichols. *J. Comp. Phys.*, 39:201, 1981.

[16] I. Steinback and F. Pezolla and B. Nestler and R. Prieler and G.J. Schmitz and J.L.L. Rezende. *Physica D*, 94:135, 1996.

[17] D. Jacqmin. Some convergence results for phase-field surface tension modeling of two-phase navier-stokes flows. In *Proc. ASME Fluids Eng. Div. Summer Mtg.*, June 1997.

[18] D. Jacqmin. Calculation of two-phase navier-stokes flows using phase-field modeling. *J. Comp. Phys.*, 155:96–127, 1999.

[19] R. Kobayashi. *Physica D*, 63:410, 1993.

[20] R. Kobayashi, J. A. Warren, and W. C. Carter. Vector-valued phase field model for crystallization and grain boundary formation. *Physica D*, 119:415–523, 1998.

[21] R. Kobayashi, J. A. Warren, and W. C. Carter. A continuum model of grain boundaries. *Physica D*, 140:141–150, 2000.

[22] C. Krill III and L. Chen. Computer simulation of 3-d grain growth using a phase-field model. *Acta Materialia*, 50:3057–3073, 2002.

[23] Y. Lu, C. Beckermann, and A. Karma. Convection effects in three-dimensional dendritic growth. In *Proc. MRS Fall Meeting*, page unknown, 2001.

[24] B. Morin, K. Elder, M. Sutton, and M. Grant. *Phys. Rev. Lett.*, 75:2156, 1995.

[25] A. Powell IV. Illuminator: A distributed visualization library for PETSc, year=2004, note=http://lyre.mit.edu/p̃owell/illuminator.html.

[26] A. Powell IV and D. Dussault. Floating solids: Combining phase field and fluid-structure interactions. *Appl. Numer. Anal. Comp. Math.*, 2(1):157–166, 2005.

[27] A. Powell IV, B. Zhou, W. Pongsaksawad, and J. Vieyra. Rheoplast, 2004. http://lyre.mit.edu/p̃owell/rheoplast.html.

[28] J. Sethian. *Level-Set Methods and Fast Marching Methods.* Cambridge University Press, 1999.

[29] X. Tong, C. Beckermann, and A. Karma. *Phys. Rev. E*, 63:061601, 2001.

[30] R. Tonhardt and G. Åmberg. *J. Crystal Growth*, 194:406–425, 1998.

[31] J. A. Warren and W. J. Boettinger. *Acta Metall. Mater.*, 43:689, 1995.

[32] J. A. Warren, R. Kobayashi, A. E. Lobkovsky, and W. C. Carter. Extending phase field models of solidification to polycrystalline materials. *Acta Mater.*, 51:6035–6058, 2003.

[33] B. Zhou and A. Powell IV. Phase field simulations of liquid-liquid demixing during immersion precipitation of polymeric membranes in 2d and 3d,. unpublished, 2005.